40-50-day Oscillation Revealed in 1963 in a Chinese Journal, Eight Years before Madden and Julian

Tim Li* (UH), Bin Wang (UH), Bill Lau (UM), Chidong Zhang (NOAA), Lu Wang (UH), Melinda Peng (NRL) and K.-C. Kuo (NTU)

***University of Hawaii and NUIST**

Li et al., 2018: A Paper on Tropical Intraseasonal Oscillation Published in 1963 in a Chinese Journal, **Bull. Amer. Meteor. Soc**. in press.

Madden-Julian Oscillation: A 40-50 day oscillation in tropics

MJO is one of most important discoveries in tropical atmosphere in 20th Century. Paper by M&J71 is one of most cited references in modern meteorology !

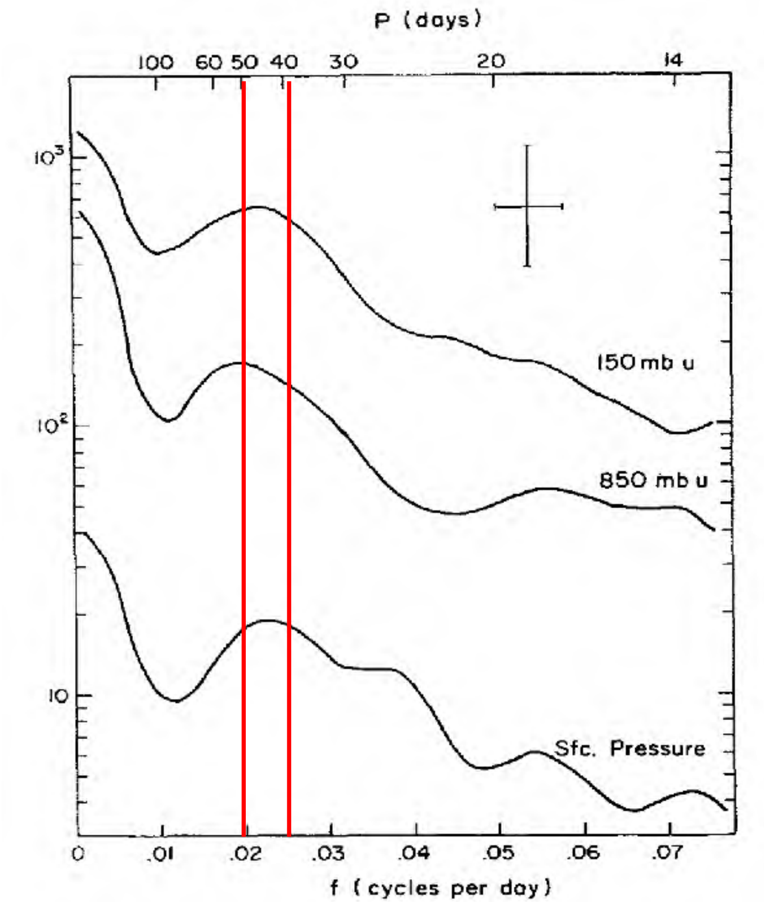

Madden and Julian, 1971

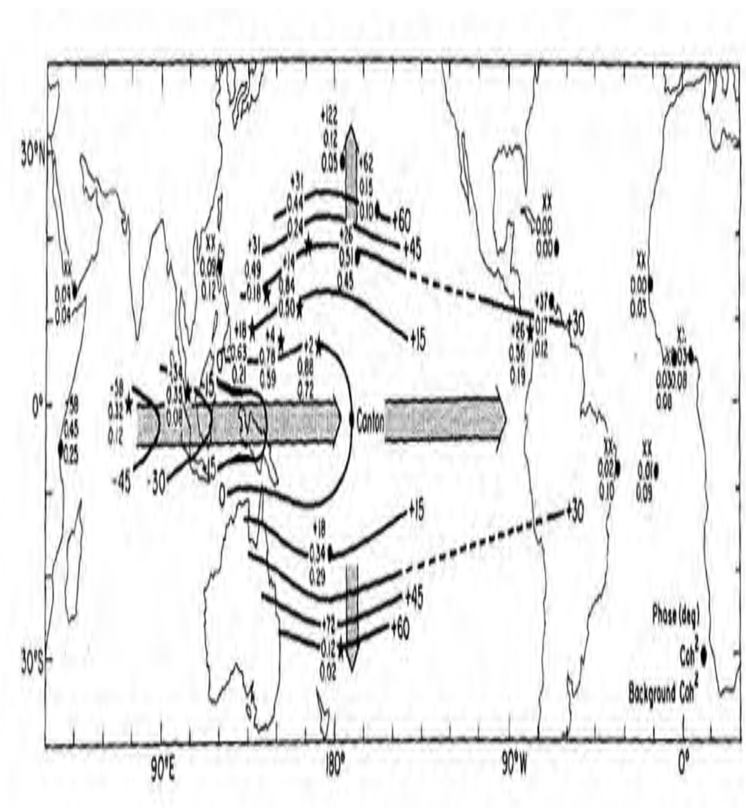

Madden and Julian, 1972

MJO Structure and Propagation Schematic (Madden and Julian 1972)

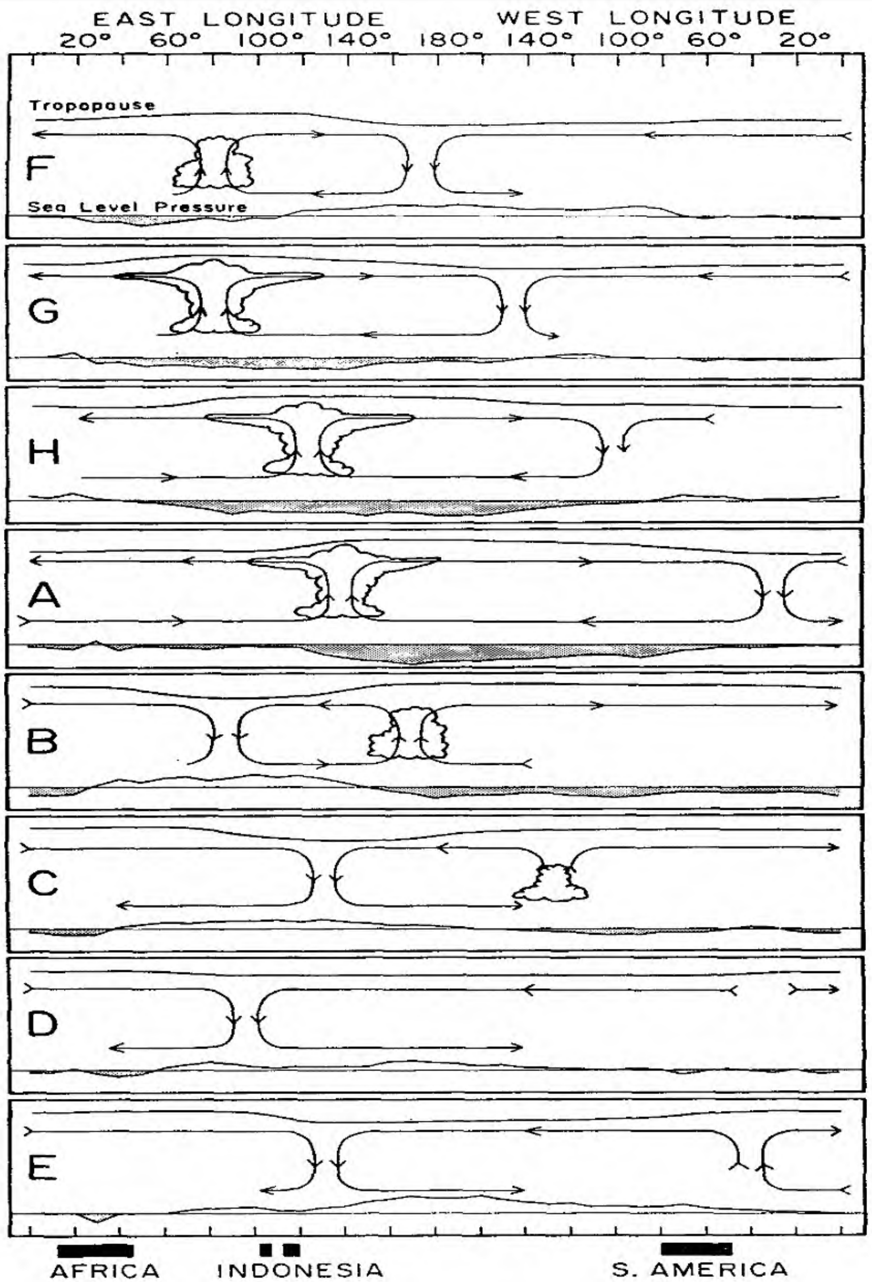

MJO Global Impacts

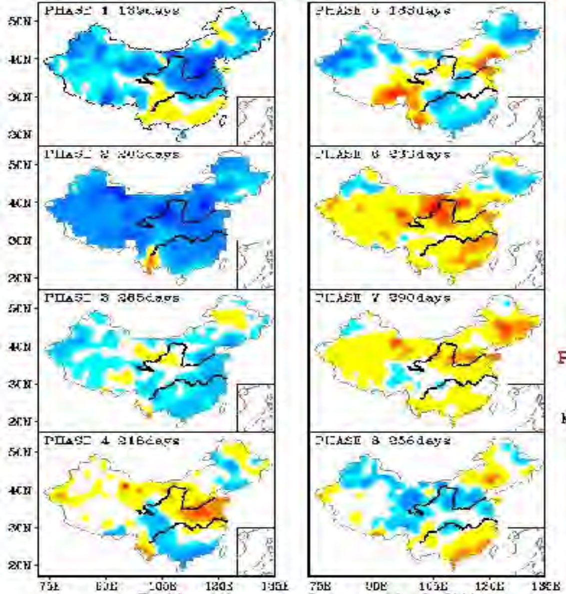

Jia et al (2010)

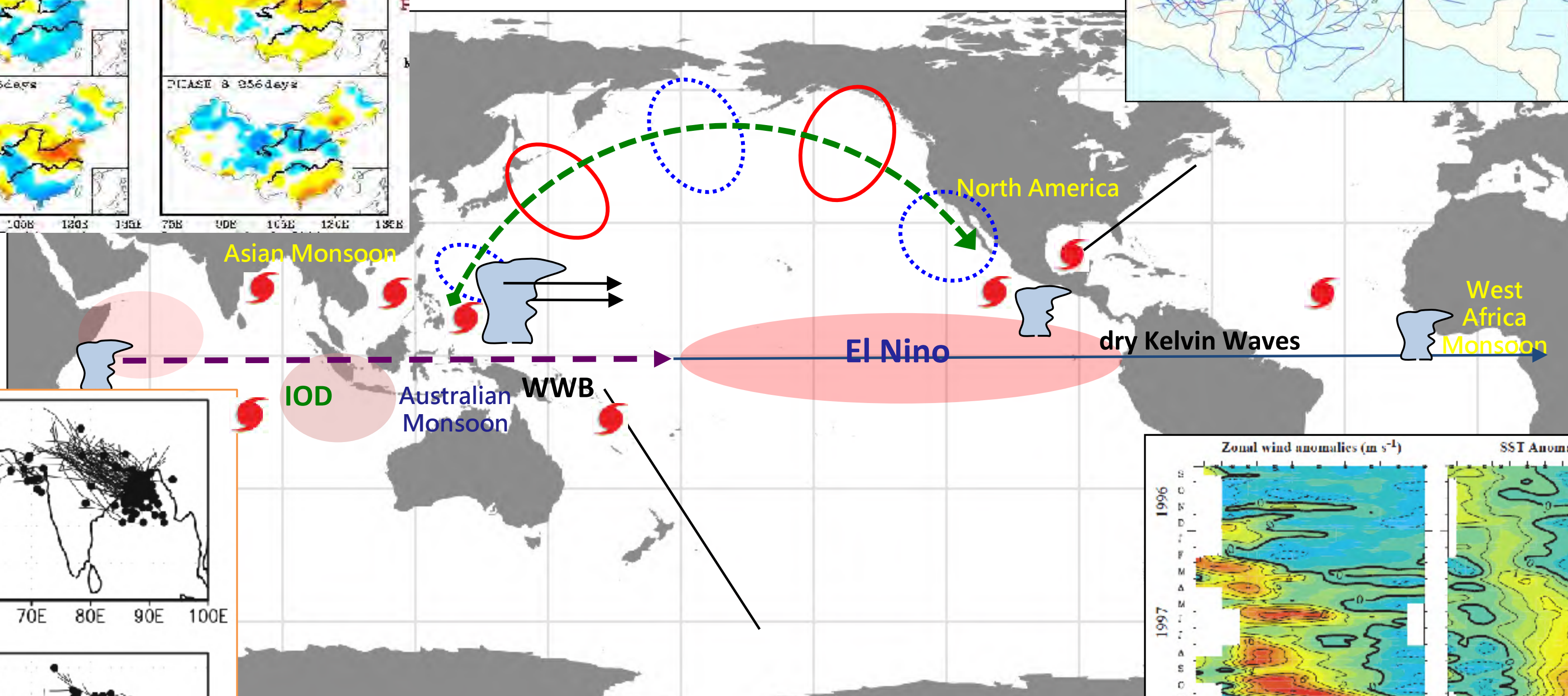

Maloney and Hartmann (2000)

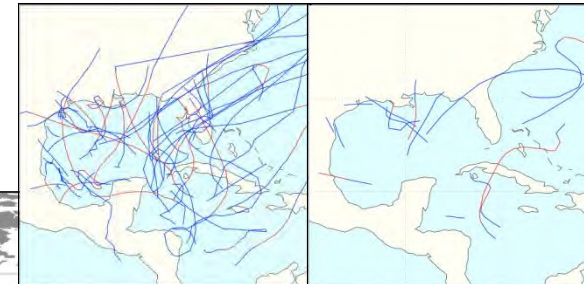

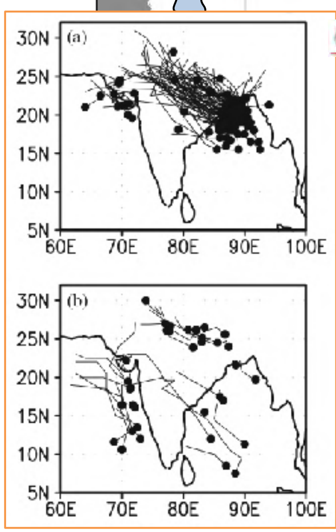

Goswami et al (2003)

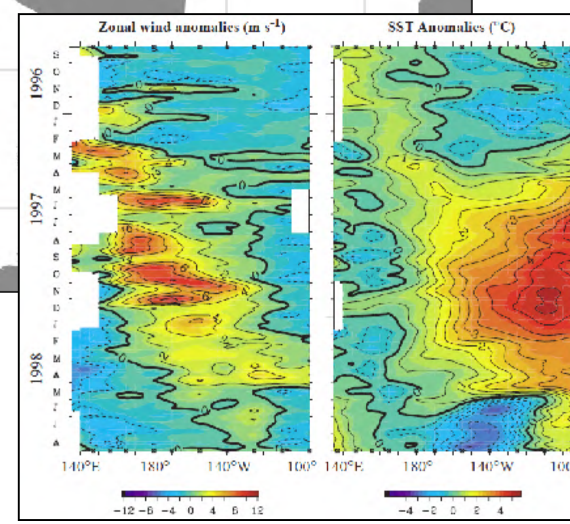

McPhaden (1999)

- Monsoon onset/break
- Tropical cyclone
- ENSO
- Mid-latitude circulation (NAO)
- Extreme weather in East Asia

Long-Persistent (23 days) Ice-Storm Events in South China

Affected Area: **10 Provinces**

Economic loss: **105 B CNY**

During Jan. 10 – Feb. 1, 2008, there were four events. CMA was able to forecast each event at a short lead, but could not predict the persistent events in advance.

Tropical MJO activity during Jan-Feb 2008

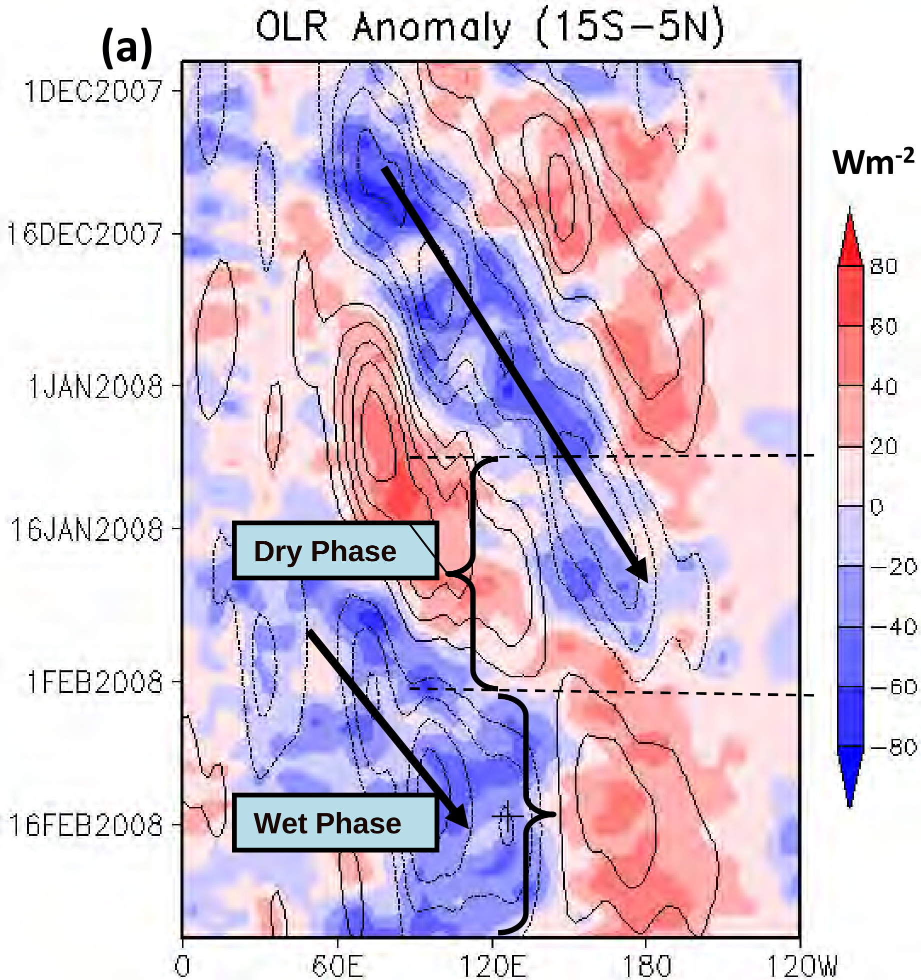

(a) The Hovmüller diagram for the daily OLR anomaly averaged over 15°-5°S. The shading denotes the raw OLR data and the contour represents 20-70-day filtered anomalous OLR.

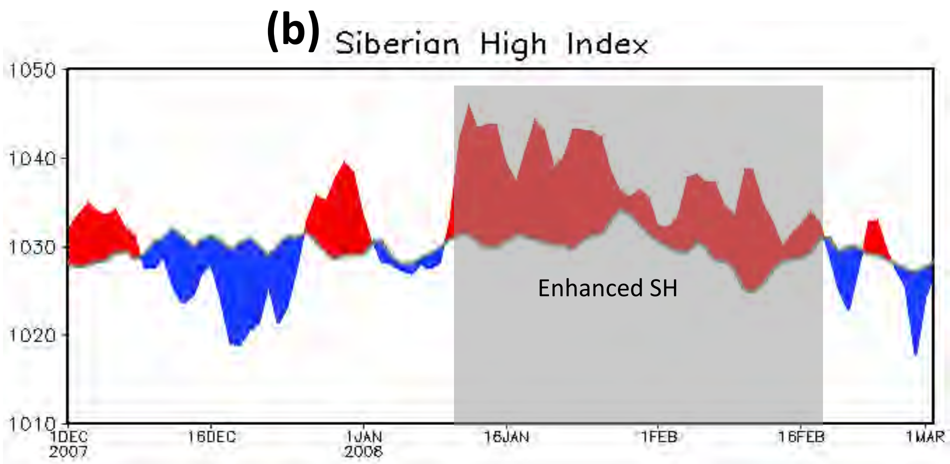

(b) Time series of the SH index (defined as the averaged SLP (hPa) over 80°-120°E, 40°-60°N). The gray shading denotes the periods of the enhanced SH.

Hong and Li, 2009, JC

Observed MJO-TC Relationship

(Liebmann et al. 1994)

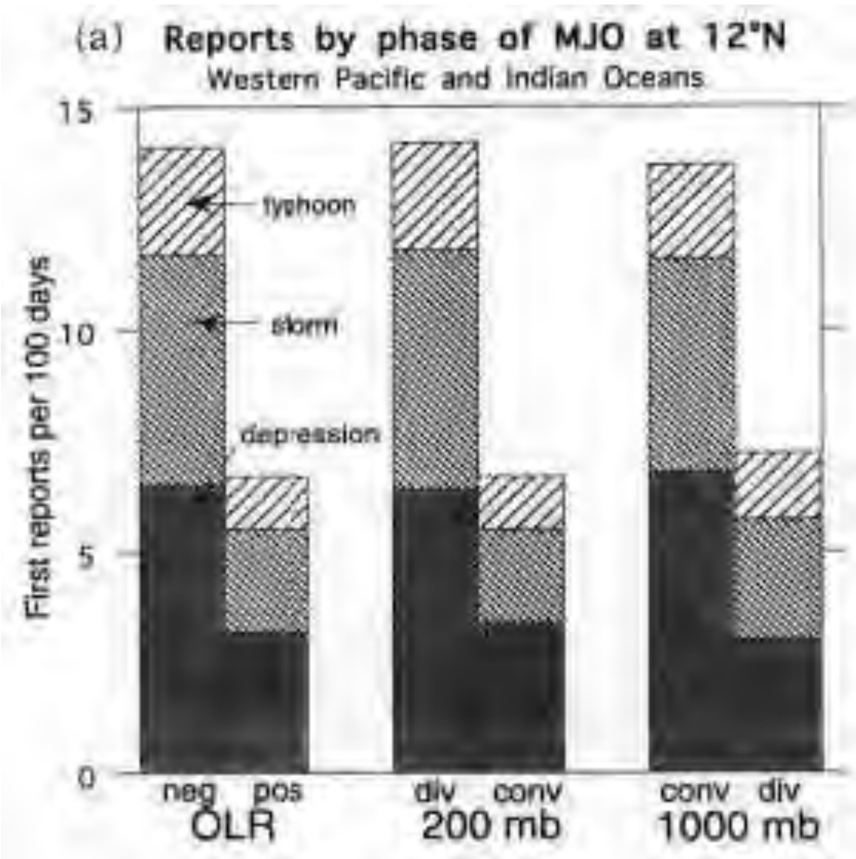

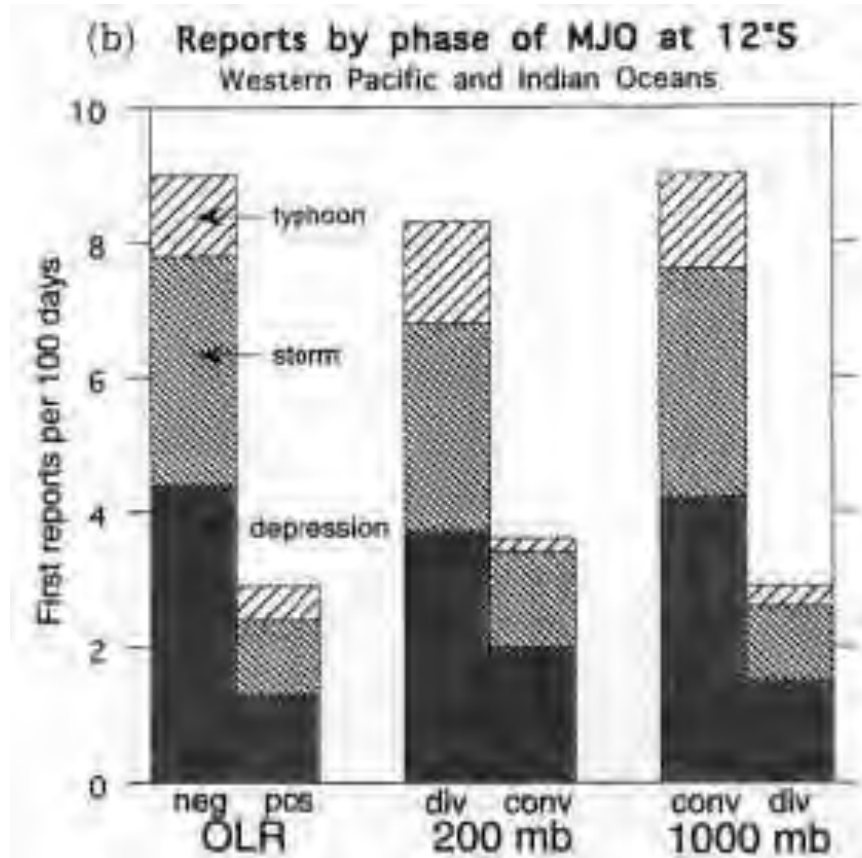

Increased (decreased) TC frequency during MJO active (inactive) phase

Eric D. Maloney, and Dennis L. Hartmann
Science 2000;287:2002-2004

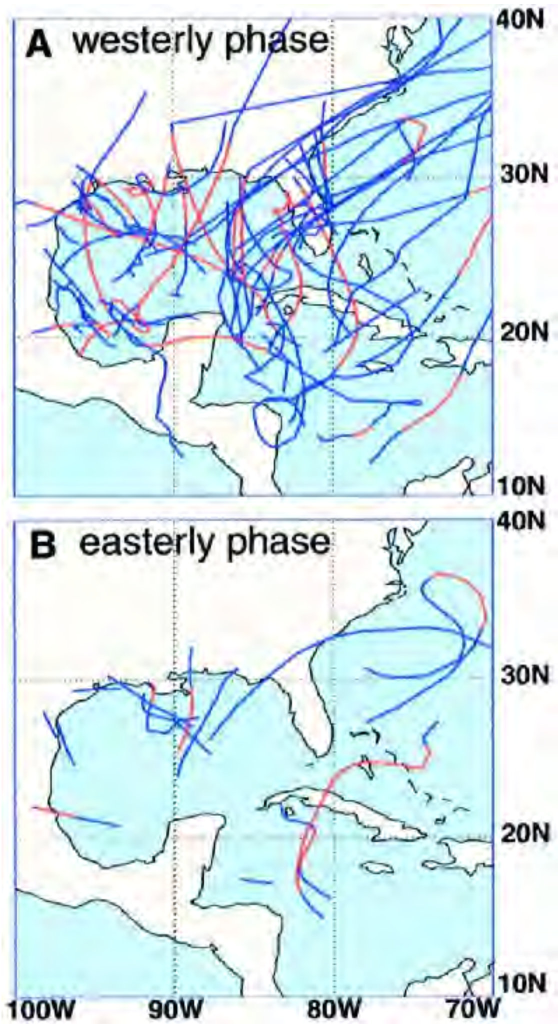

Figure 2 Tracks of Gulf of Mexico, Caribbean Sea, and western Atlantic tropical cyclones that form to the west of 77.5°W when the MJO index has a magnitude greater than 1 SD from zero.

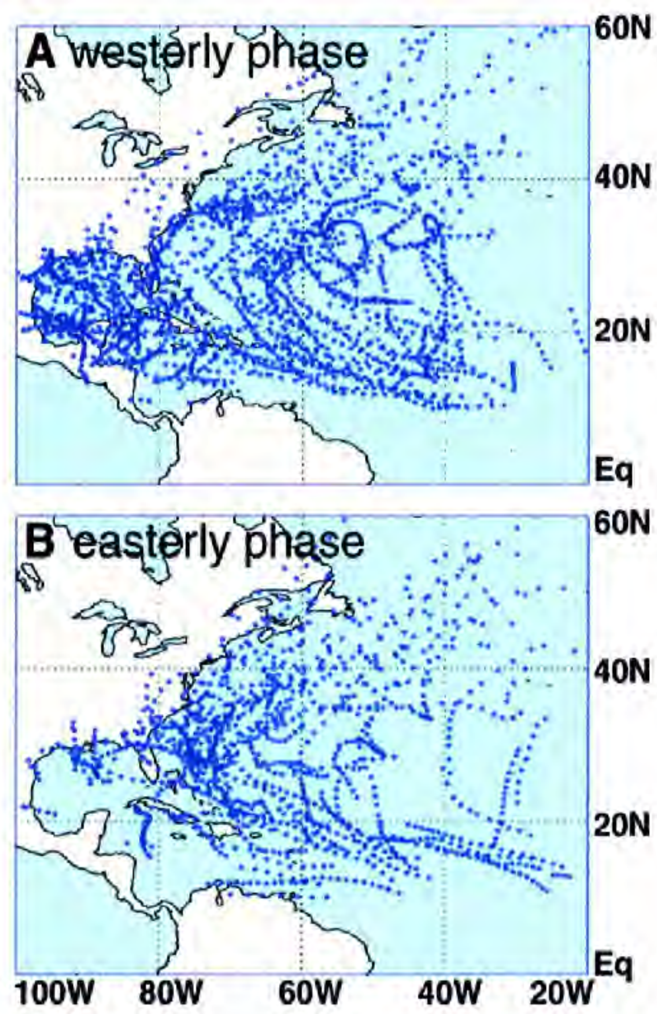

Figure 4 Atlantic tropical storm and hurricane positions during westerly (greater than 1 SD) (A) and easterly (less than −1 SD) (B) MJO phases.

WCRP: Seamless Weather-Climate Prediction

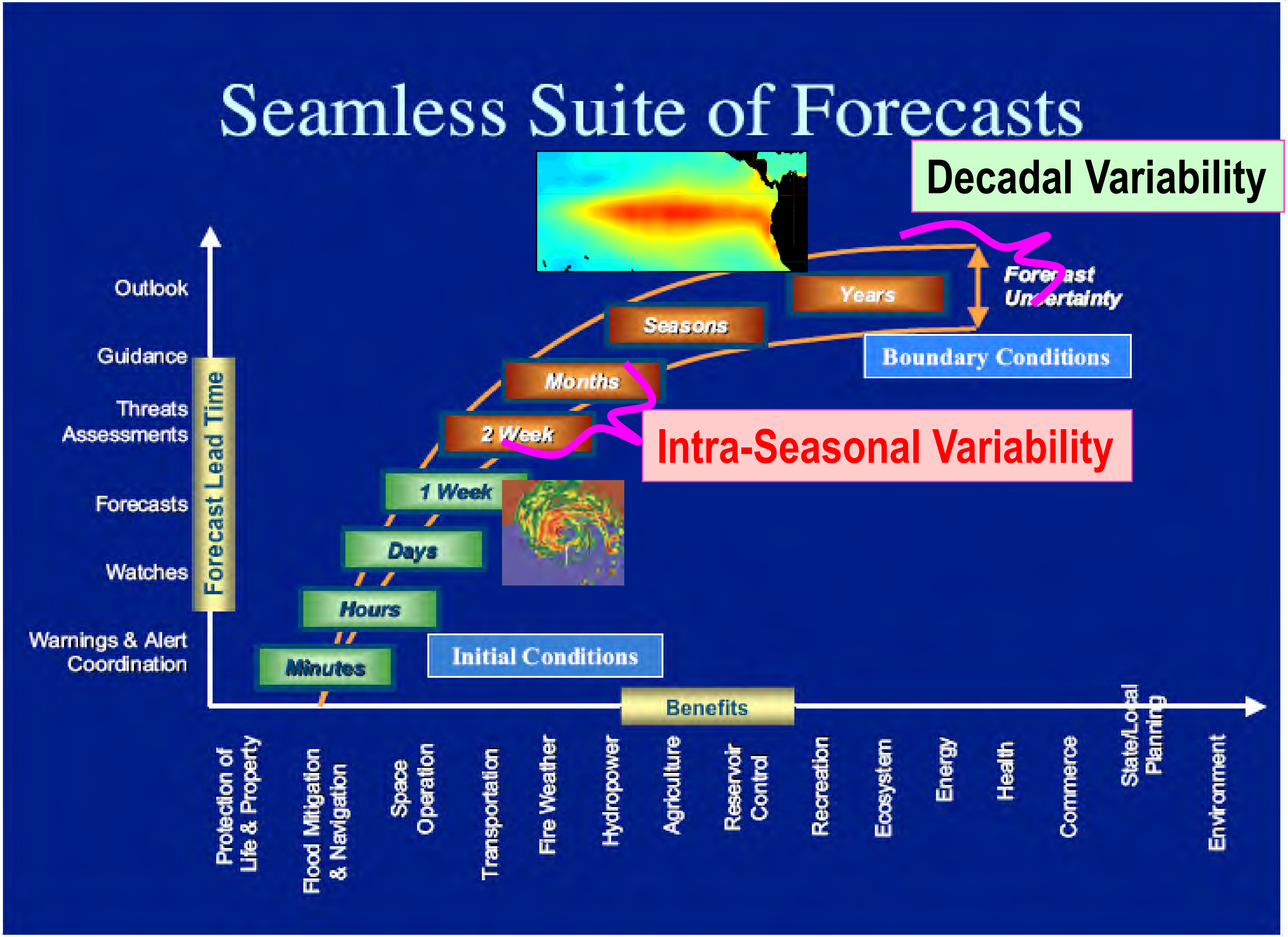

International Observational Campaign

DYNAMO/CINDY (Oct 2011 - Jan 2012)

Objective: Understanding MJO initiation mechanism

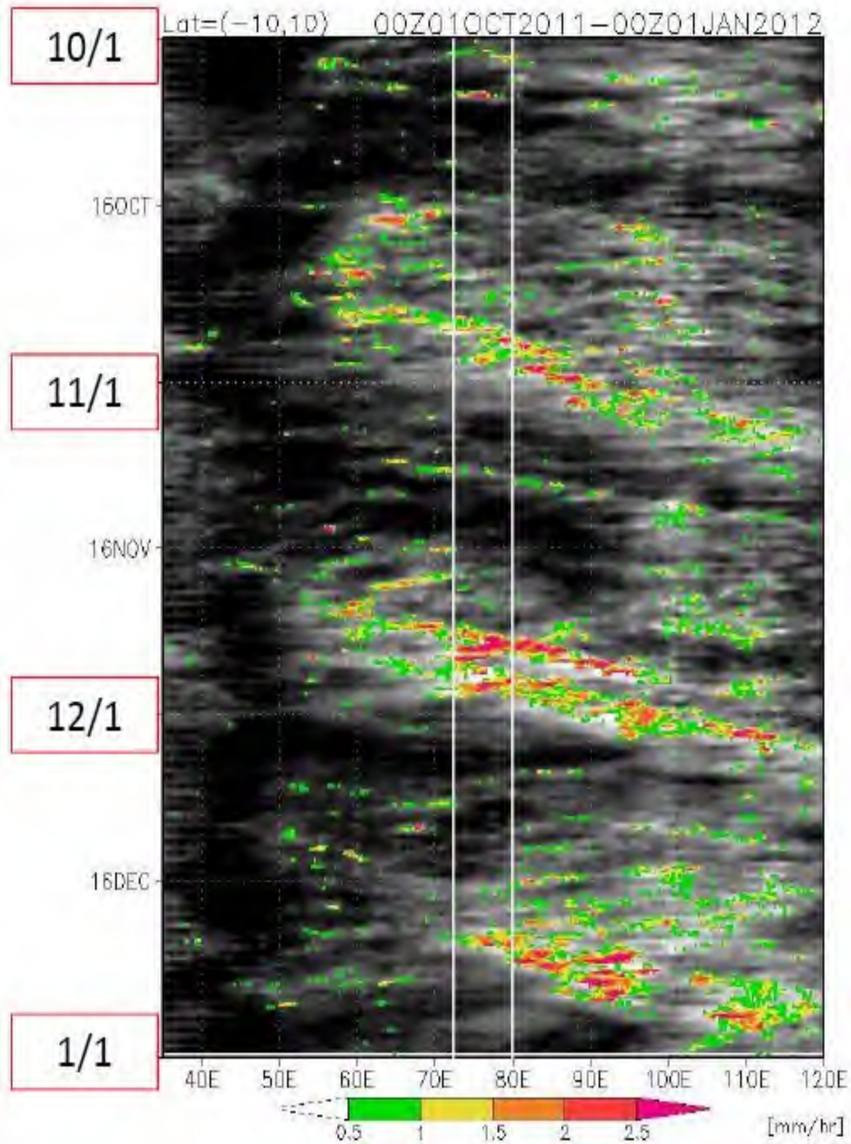

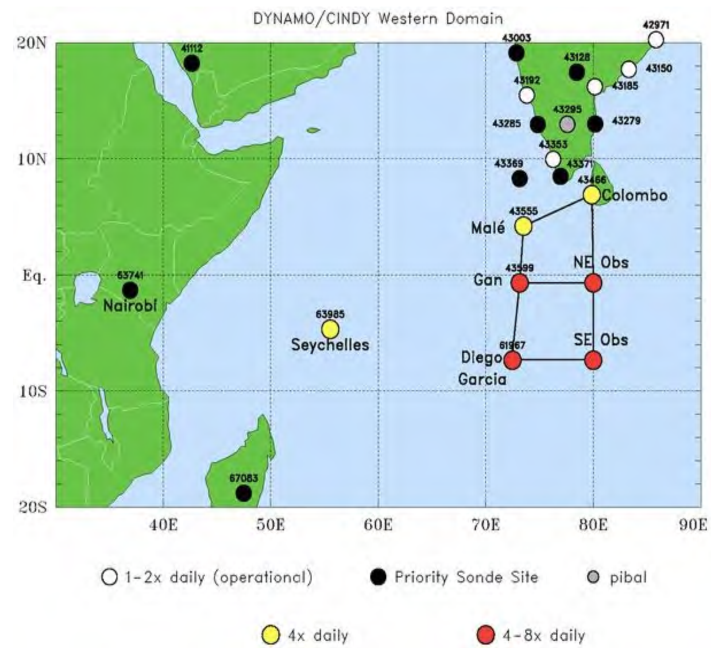

Left: Time-longitude section of unfiltered rainfall field along the equator (averaged at 10S-10N)

Top: **3-hourly intensive observational networks** (two ships, two island stations)

Xie et al. (1963) (hereafter Xie63) discovered a 40-50-day period oscillation in zonal wind over southeast Asian monsoon domain, published in a Chinese meteorological journal in 1963, 8 years earlier than M&J (1971).

Xie et al., 1963: Relation between the Southeast Asian Basic Flow and Typhoon Occurrence – Statistics and Analysis. *ACTA Meteorologica Sinica*, Vol 33, No 2, May 1963

Radiosonde Stations Examined by Xie et al (1963)

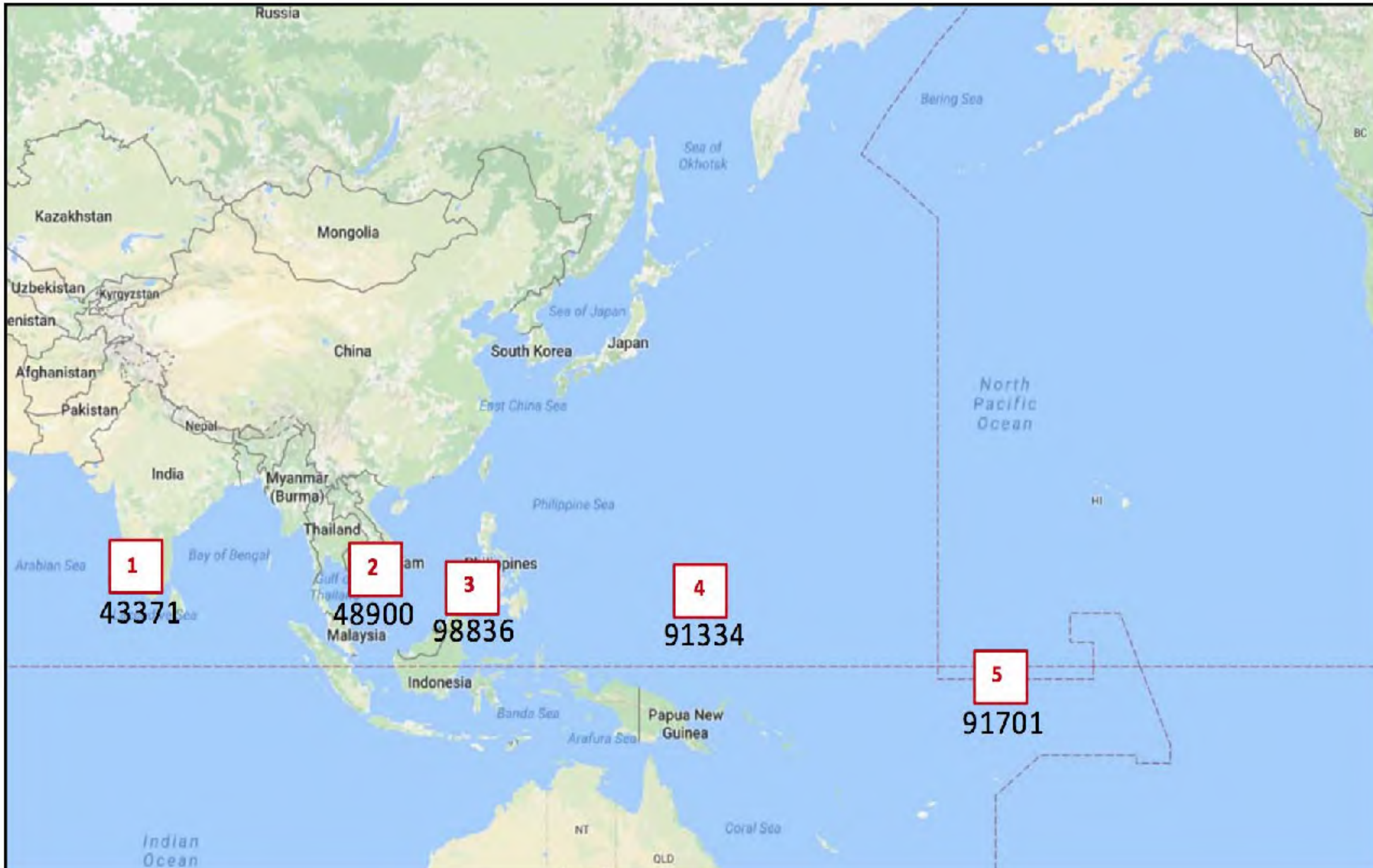

Station 5 on Canton Island was used by Madden and Julian (1971).

Westerly Wind Oscillations over Stations 371, 900 and 836 (Xie et al. 1963)

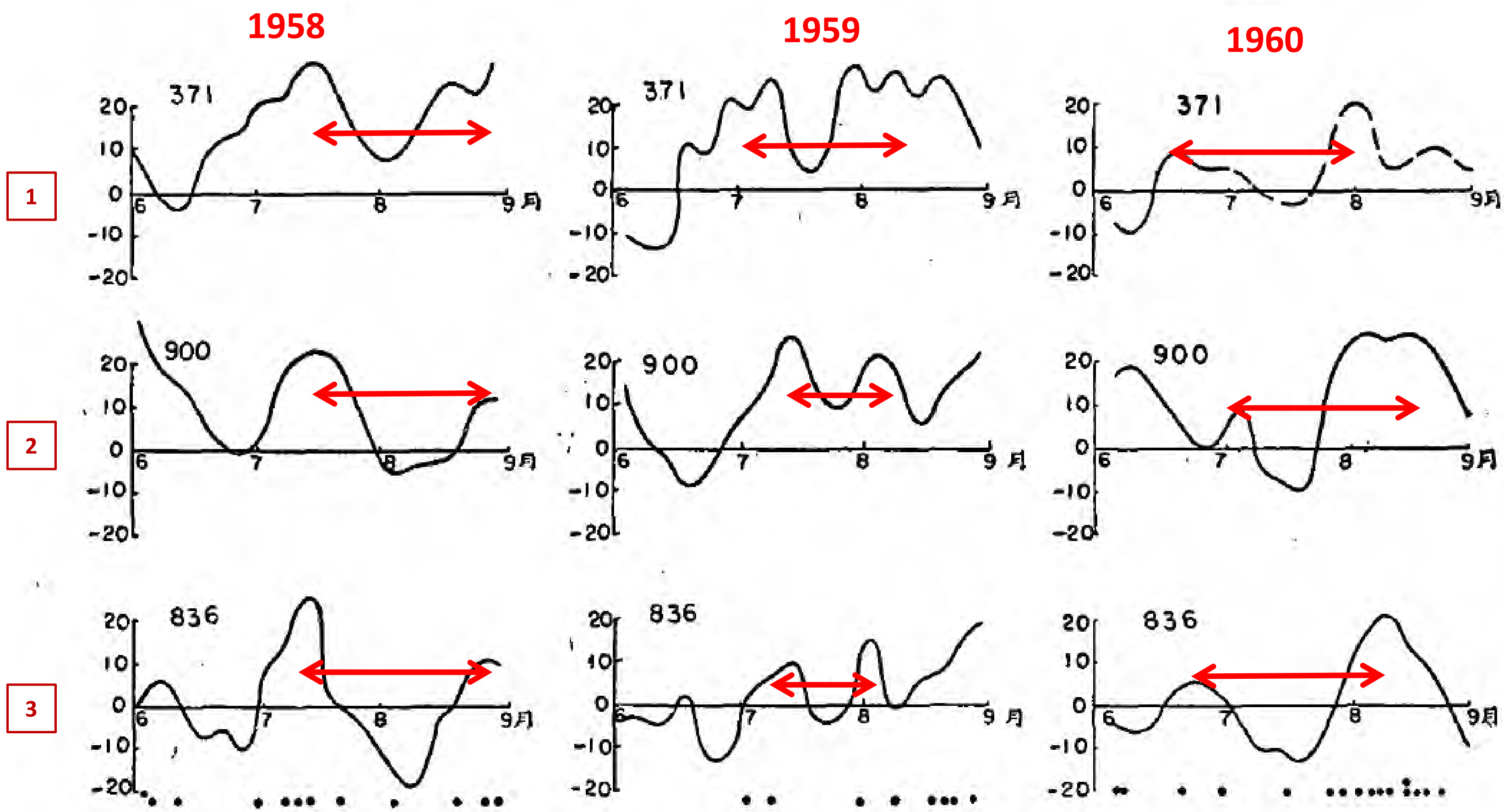

图 2 371，900 和 836 站 700 毫巴五天平均东西向风速与台风发生日期
正値为西风，負値为东风，单位：米/秒，黑点为台风发生日期

Original Fig. 2 from Xie et al. (1963), who indicated a one and half month period for the summer westerly variation in the monsoon region.

Comparing Xie63 hand-draw result with station soundings and NCEP reanalysis

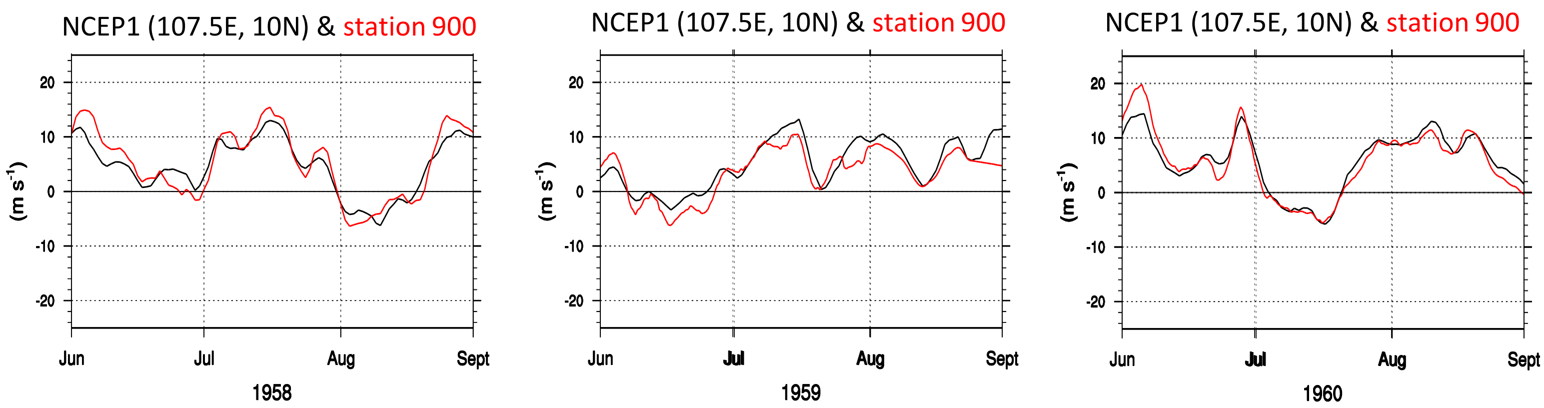

Xie et al (1963) for 1958 at station 900

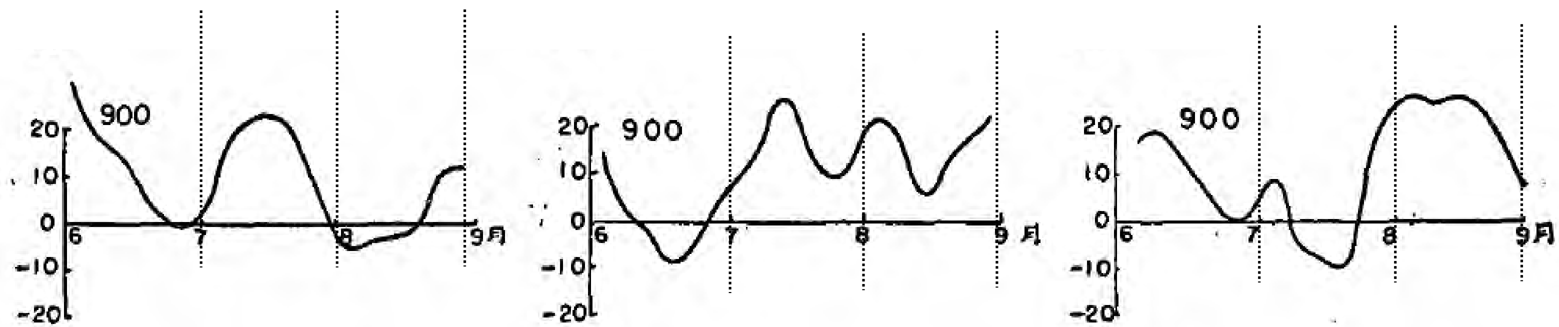

Xie's hand-draw figures are confirmed by archived soundings and modern reanalysis data.

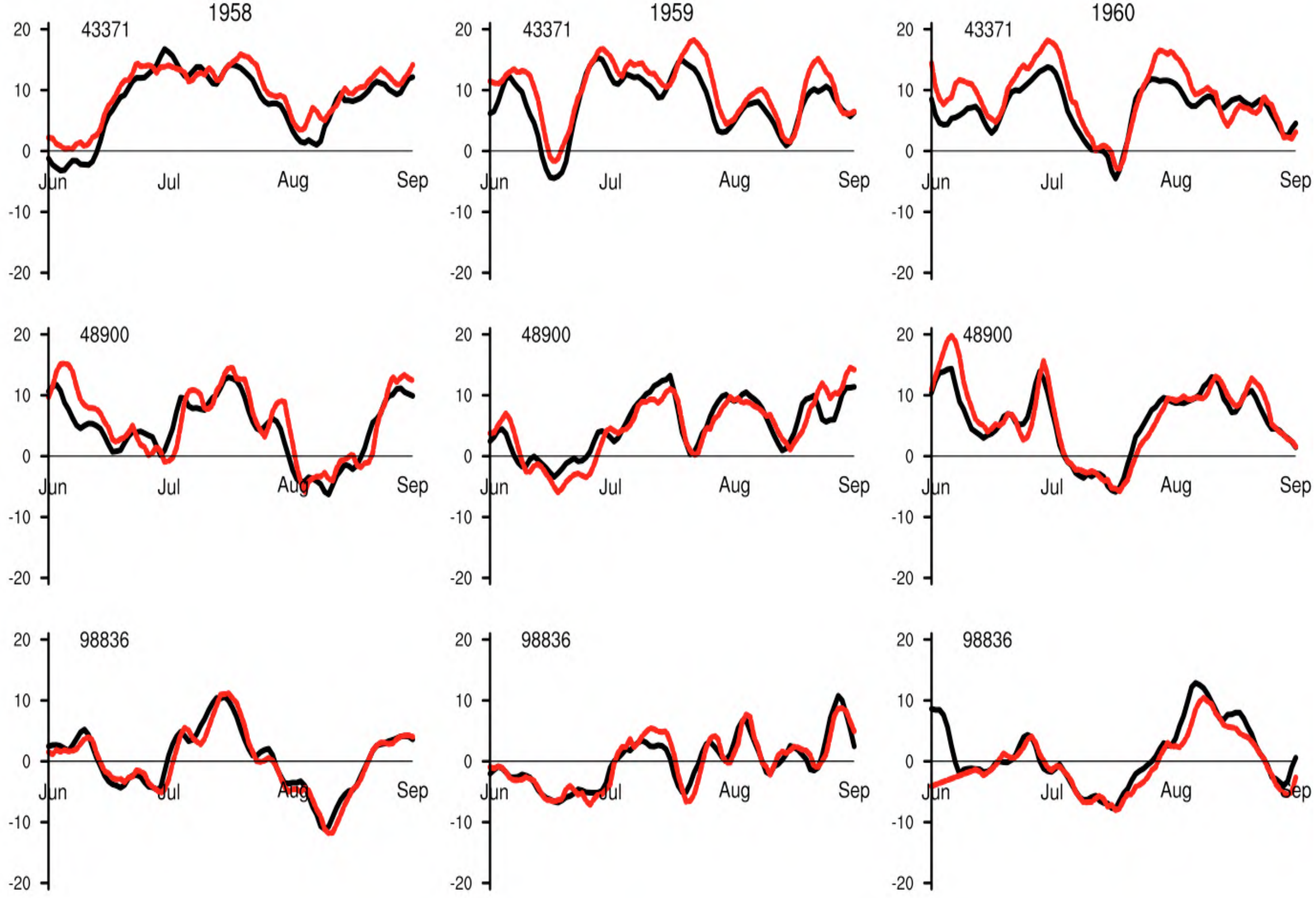

Time series of 700-hPa 5-day running mean zonal wind (m s^{-1}) from June 1 to September 1 in 1958, 1959 and 1960. Red curves are from archived station radiosonde data, and black curves are from nearby NCEP grid point data.

Power Spectrum Analysis of Zonal Wind (1958-1970)

Variance spectra for zonal wind (m^2 s^{-2}) at 150 hPa (blue solid), 700 hPa (black solid) and 850 hPa (red solid) for Station (a) 43371, (b) 48900, and (c) 91701 during **1958-1970**.

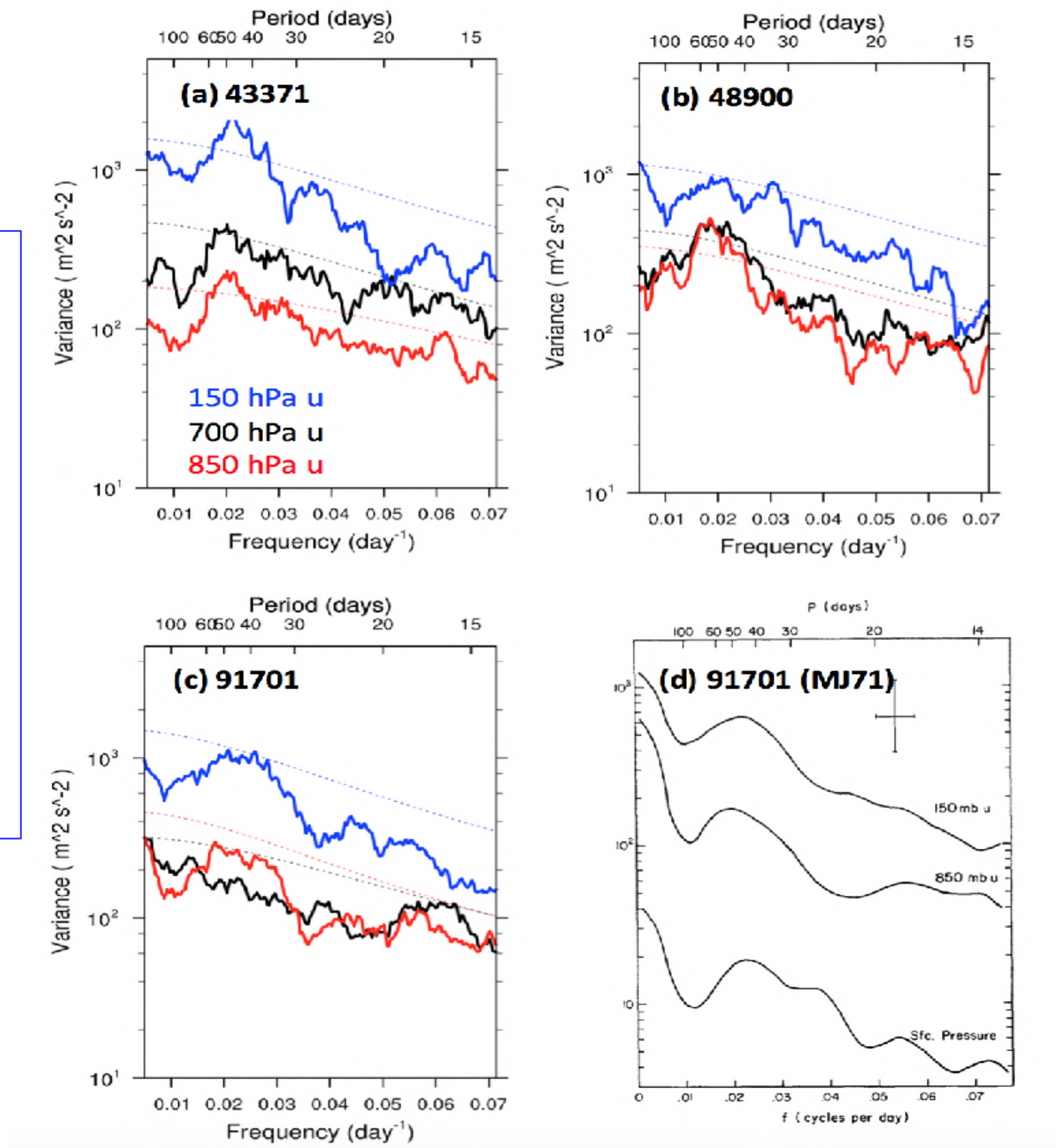

Dotted lines mark the 95% confidence level

(d) is original Fig. 2 of M&J71

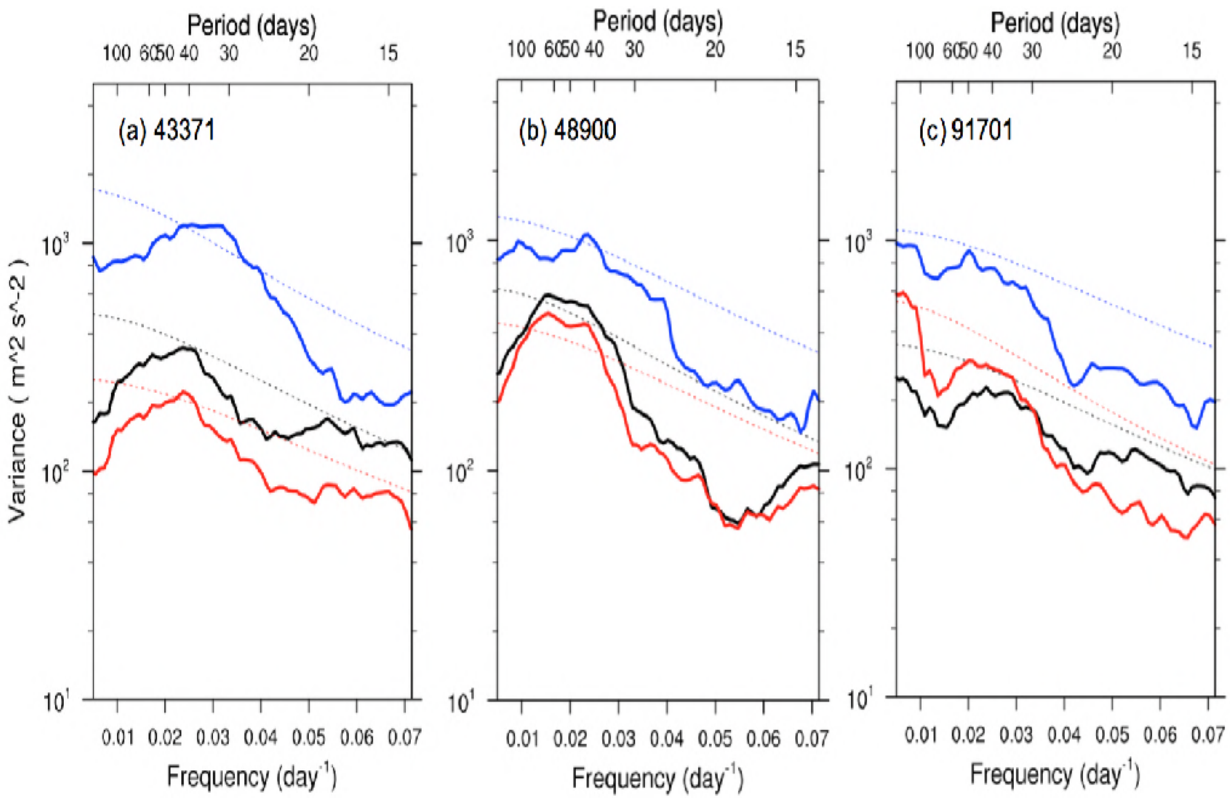

Variance spectra for zonal wind (m^2 s^{-2}) at 150 hPa (blue solid), 700 hPa (black solid) and 850 hPa (red solid) for Station 43371, 48900, and 91701 during the three-year (1958-1960) period studied by Xie63. Dotted lines mark the 95% confidence level.

Vertical Distribution of 40-50-day Oscillation at 5 Stations

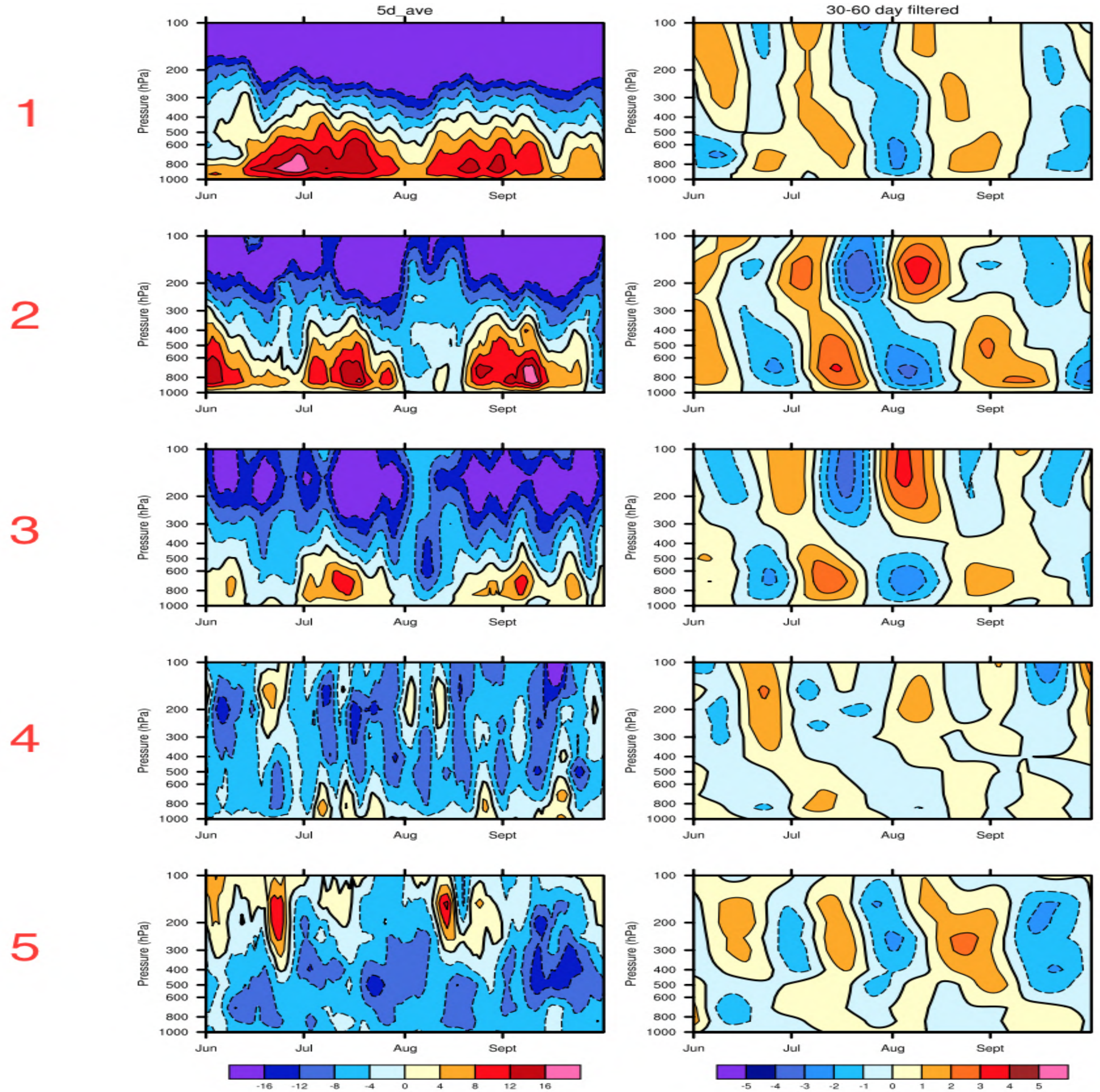

Co-Spectrum between 850-hPa and 150-hPa Zonal Wind and Coherence-Squared Statistic

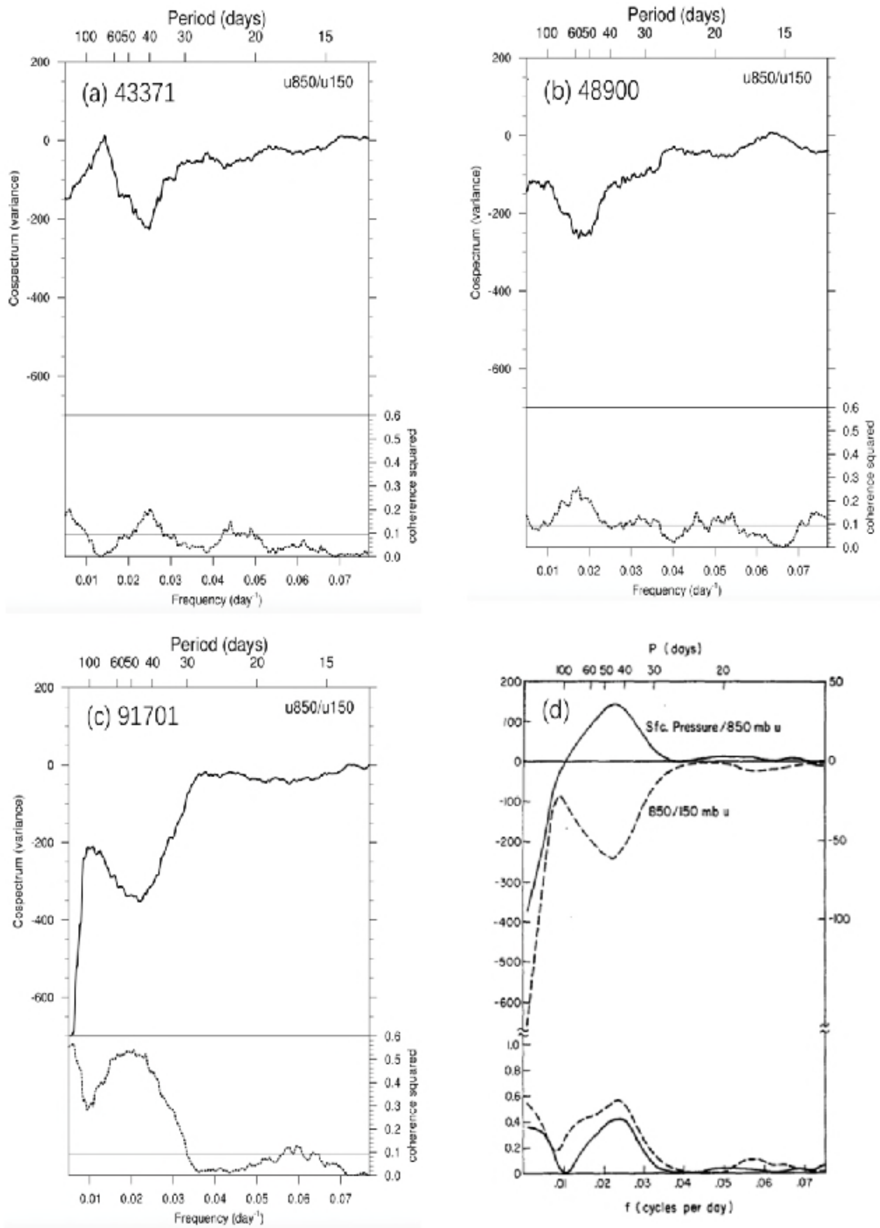

Co-spectrum between 850-hPa and 150-hPa zonal wind ($m^2\ s^{-2}$) during 1958-1970 (**top curves**) and **coherence-squared statistic** for 850-hPa and 150-hPa zonal wind (**bottom curves**) at Station (a) 43371, (b) 48900, and (c) 91701. The 95% confidence level is denoted by the thin line. The original Fig. 1 from MJ71 is shown in (d) in comparison to the current analysis at Station 91701 (c).

Origin of the 40-50-day Zonal Wind Oscillation (1958-70)

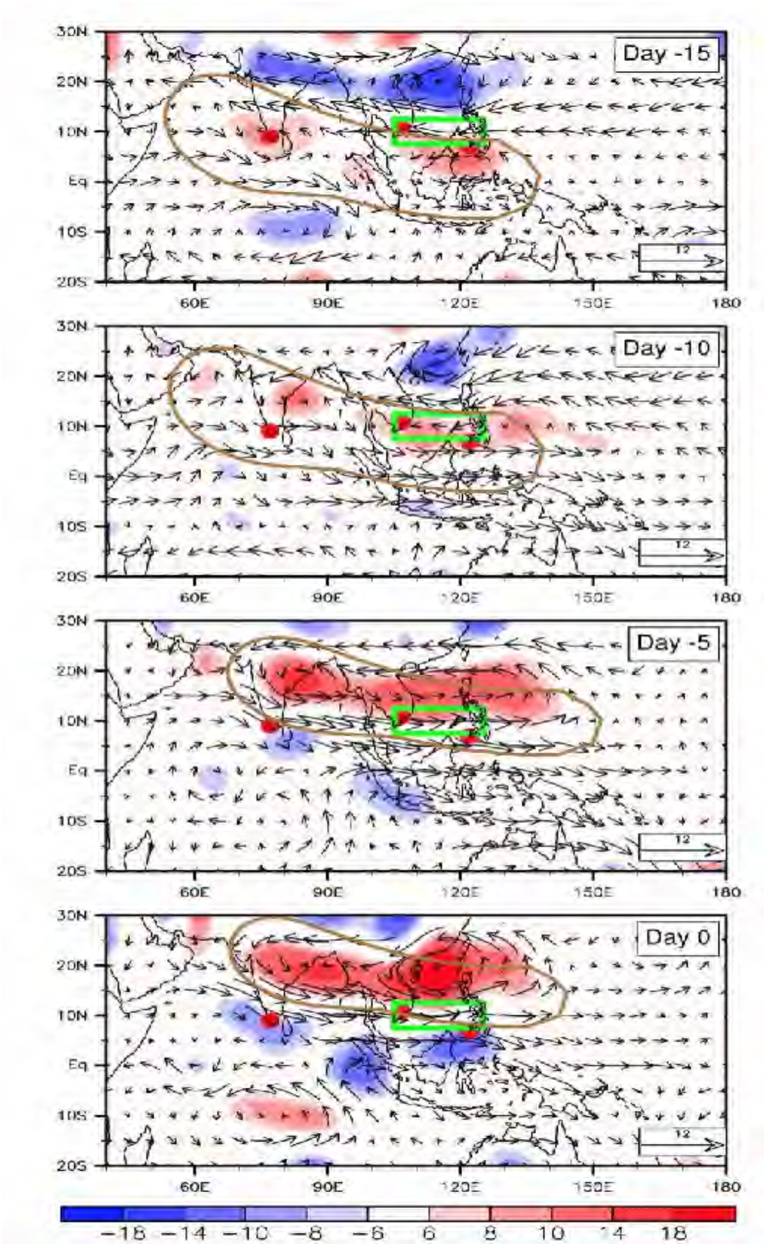

Lagged regression patterns of 30-60-day filtered 700-hPa wind anomalies (vectors, m s^{-1}) and vorticity anomaly (shading, 10^{-6} s^{-1}) against 30-60-day filtered zonal wind anomalies averaged over the reference box (7.5° N-12.5° N, 105° -125° E) (marked in green) for the period of June-September, **1958-1960**. Brown curves are hand drawn to mark the anomalous large-scale cyclonic circulation.

More Frequent TC Formation in Westerly Phase

Xie et al. (1963)

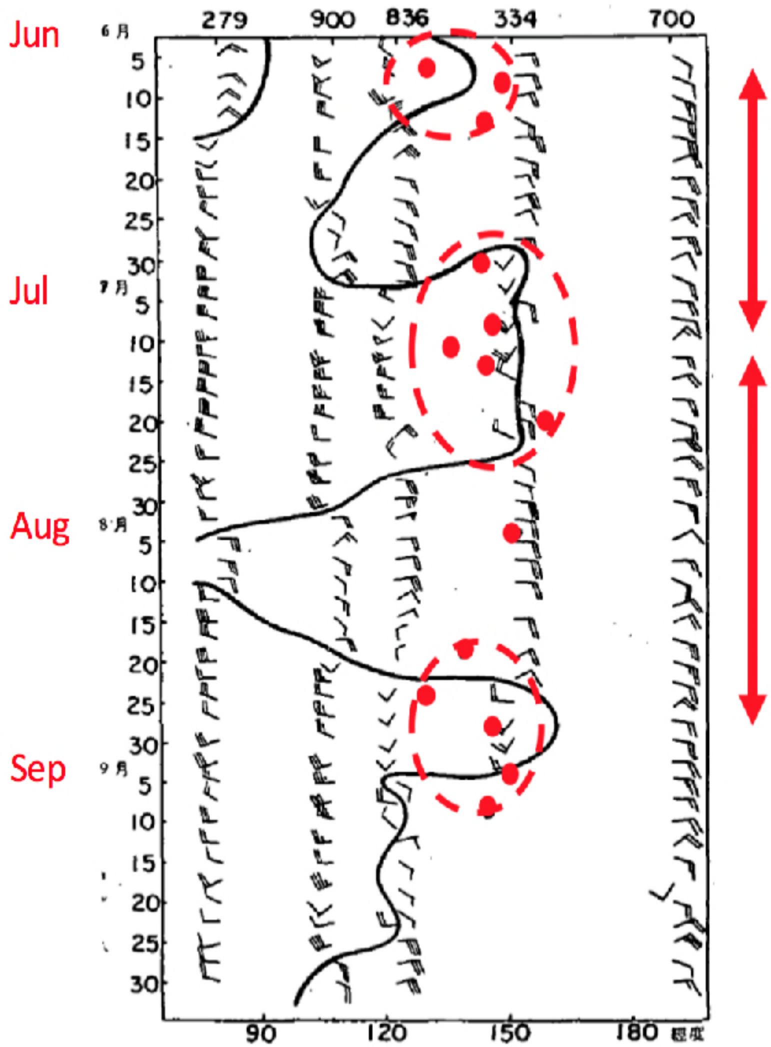

图 3 1958 年 6—9 月 印度南端到太平洋赤道附近 700 毫巴东西风分界綫与台风发生的关系

TC often formed near the confluence zone where monsoon westerly meets trade easterly.

Westerly Phase vs. Typhoon Occurrence at Stations 371, 900 and 836 (Xie et al. 1963) in 1958-1960

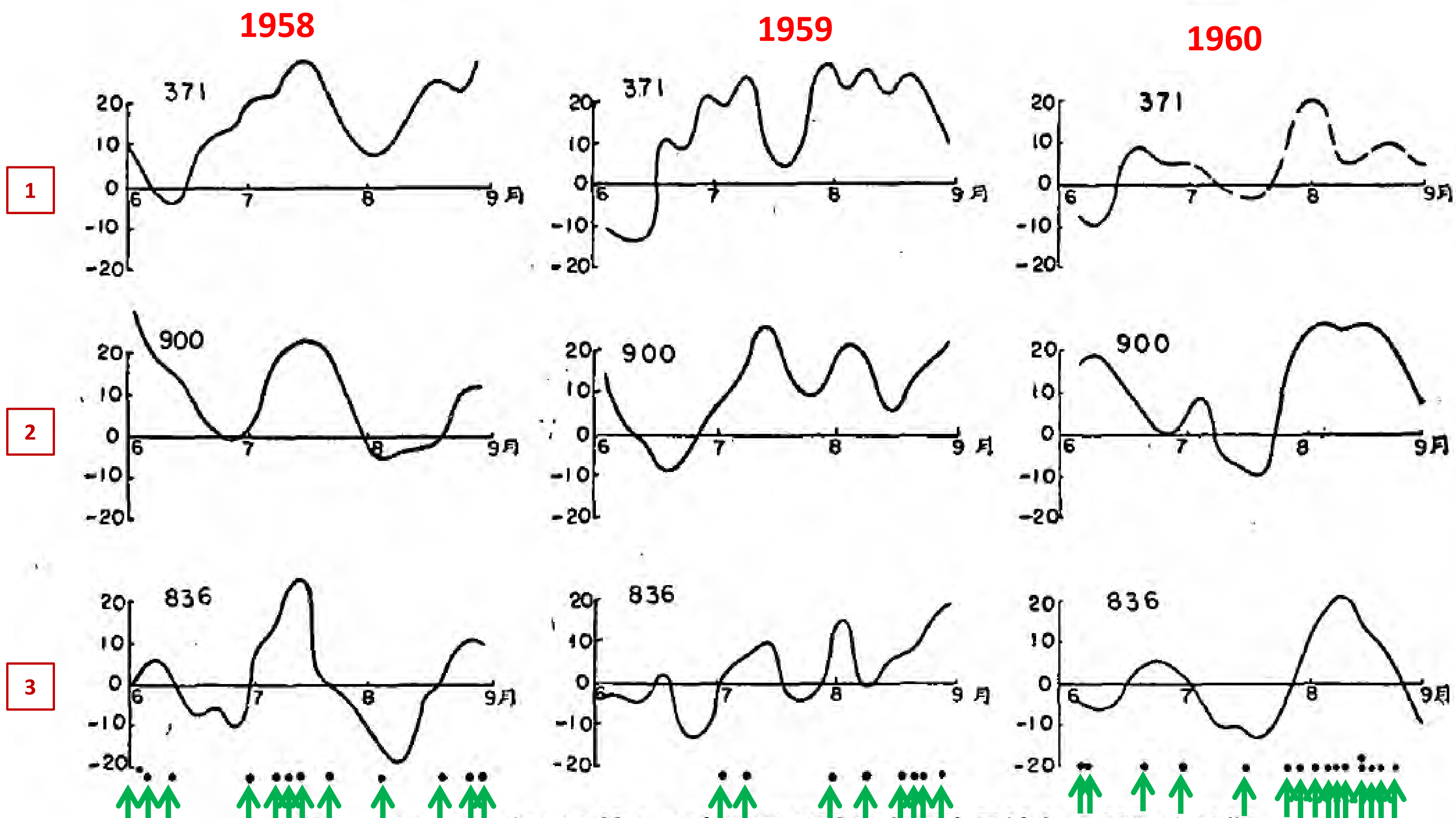

图 2　371，900 和 836 站 700 毫巴五天平均东西向风速与台风发生日期

正値为西风，負値为东风，单位：米/秒，黑点为台风发生日期

↑ Occurrence of typhoon

Composite of 20-60 day filtered 700-hPa wind anomalies (vector), rainfall anomalies (shading) and TC genesis (dotted) in JJAS during 1958-1970

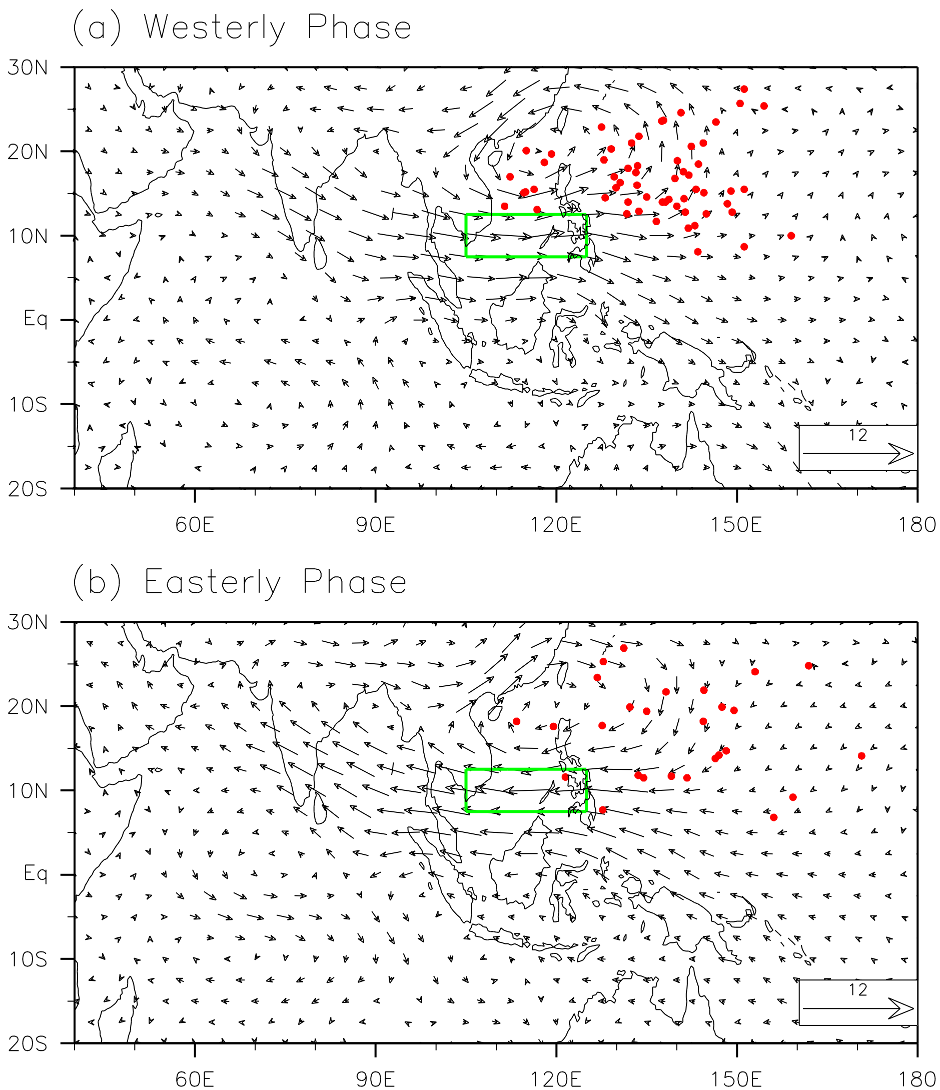

Composite patterns of 30-60-day filtered 700-hPa wind anomaly (vectors, m s^{-1}) and TC genesis location (dotted) for (a) MJO westerly phase and (b) MJO easterly phase in June - September during 1958-1970

TC genesis frequency is positively correlated with westerly phase of ISO in the WNP.

30 years later, people started to notice a close relation between TC Genesis and MJO active/inactive phase !

Hartmann et al. (1992)

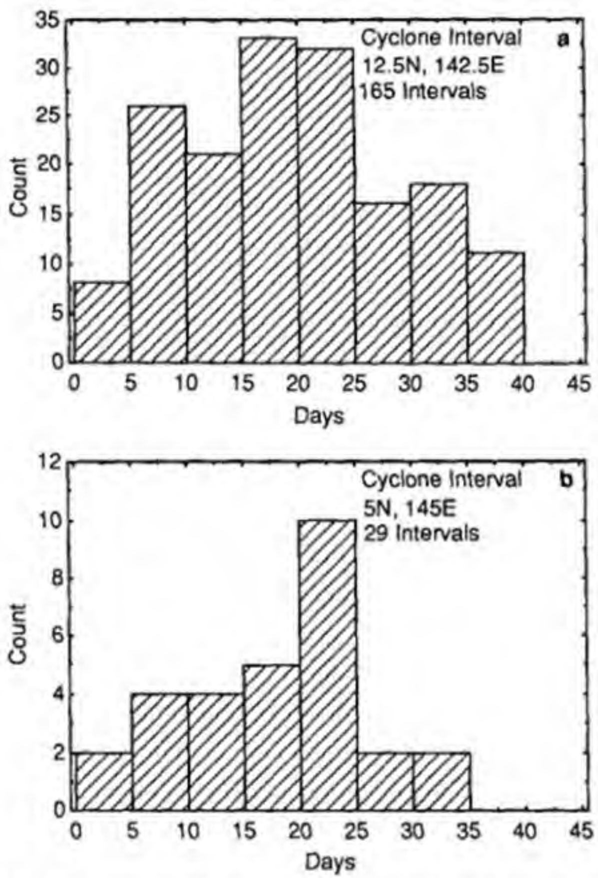

FIG. 10. Histogram for the recurrence interval between cyclones with wind speeds in excess of 64 kt, during the September–December season, and (a) within the 20-degree circular region centered at 12.5°N, 142.5°E, or (b) within the 20-degree circular region centered at 5°N, 145°E.

Liebmann, et al. (1994)

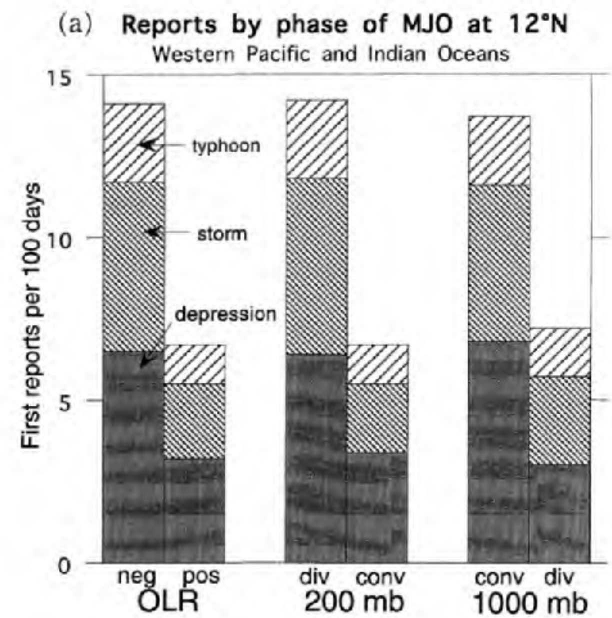

Fig. 3. (a) Number of first reports of depressions, storms, and typhoons that occur per 100 days in the MJO active and inactive phases.

Summary

1. A 40-50-day oscillation in zonal wind was first discovered by Xie et al. (1963) in the Southeast Asian monsoon domain, **eight years** before M&J71. The signal is so strong that one can identify the oscillation without filtering.

2. Typhoon genesis occurs more frequently in the western Pacific during the westerly phase of the 40-50-day oscillation. This discovery by Xie63 was about **3 decades earlier** than Hartmann et al. (1992) and Liebmann et al. (1994).

Should we call the oscillation Xie Oscillation, or Xie-Madden-Julian Oscillation (XMJO)?

With meteorology as a science that impacts people's living globally and is pursued by people everywhere, there must exist many hidden gems published in early days in non-English journals that were unknown beyond their countries. This current paper serves the purpose of bringing one of such gems and encourages others to do the same.

How does the ISO influence TC genesis in the WNP?

– Impact on synoptic-scale disturbances
– Barotropic eddy kinetic energy (EKE) conversion
– Change of background mean vorticity and humidity

Dominant Synoptic Mode in WNP – Synoptic Wave Train

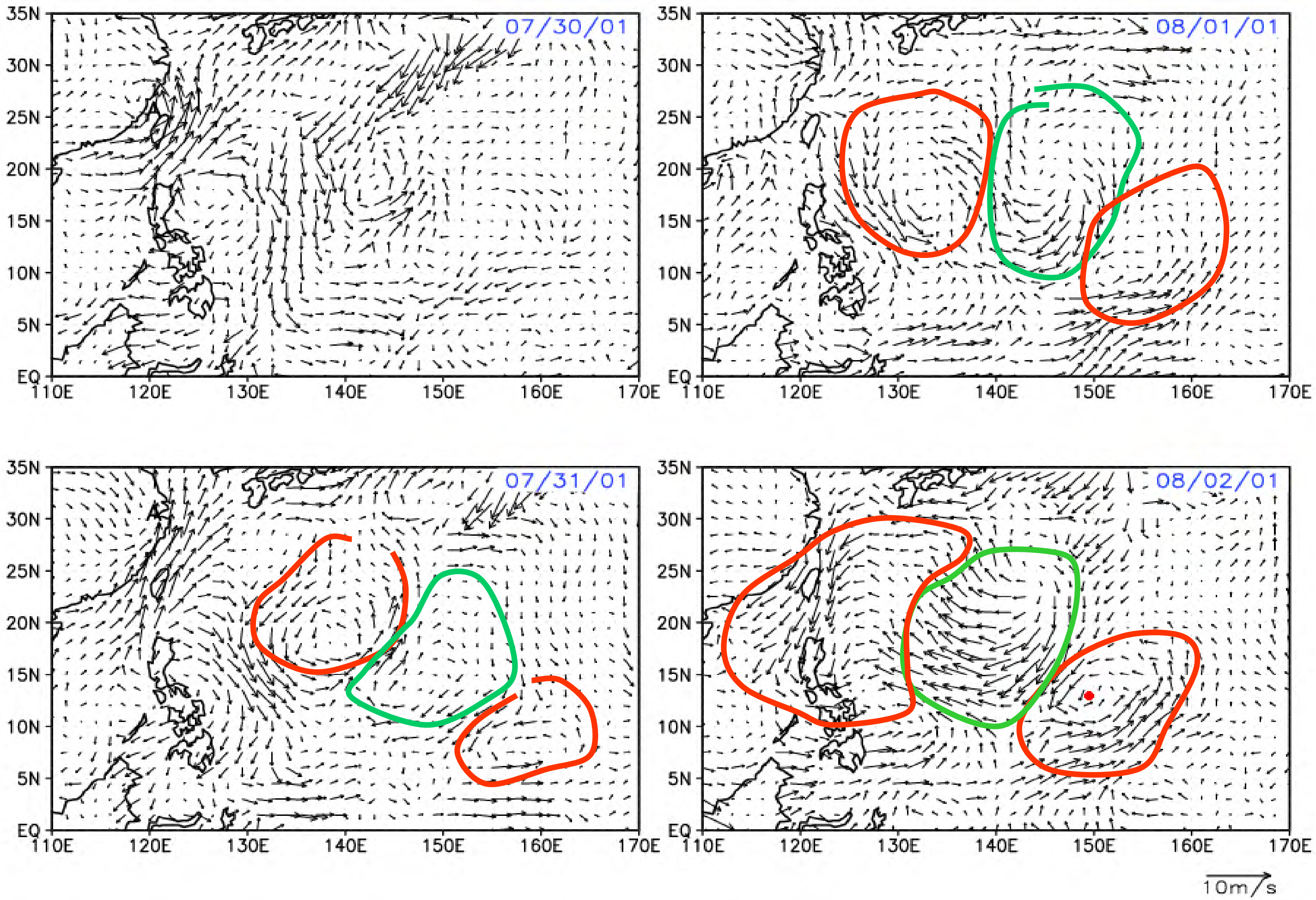

Red circle: **Cyclonic**

Green circle: **Anti-cyclonic**

- Man-yi

Time sequences of synoptic-scale surface wind patterns associated with synoptic wave train (SWT). Red dot indicates the center location of typhoon "Man-yi" at the day of genesis.

Fu, Li, et al. 2007

Synoptic 850hPa wind (vector) and vorticity (contour) during ISO wet (left) and dry (right) phase (Zhou and Li 2010, JC)

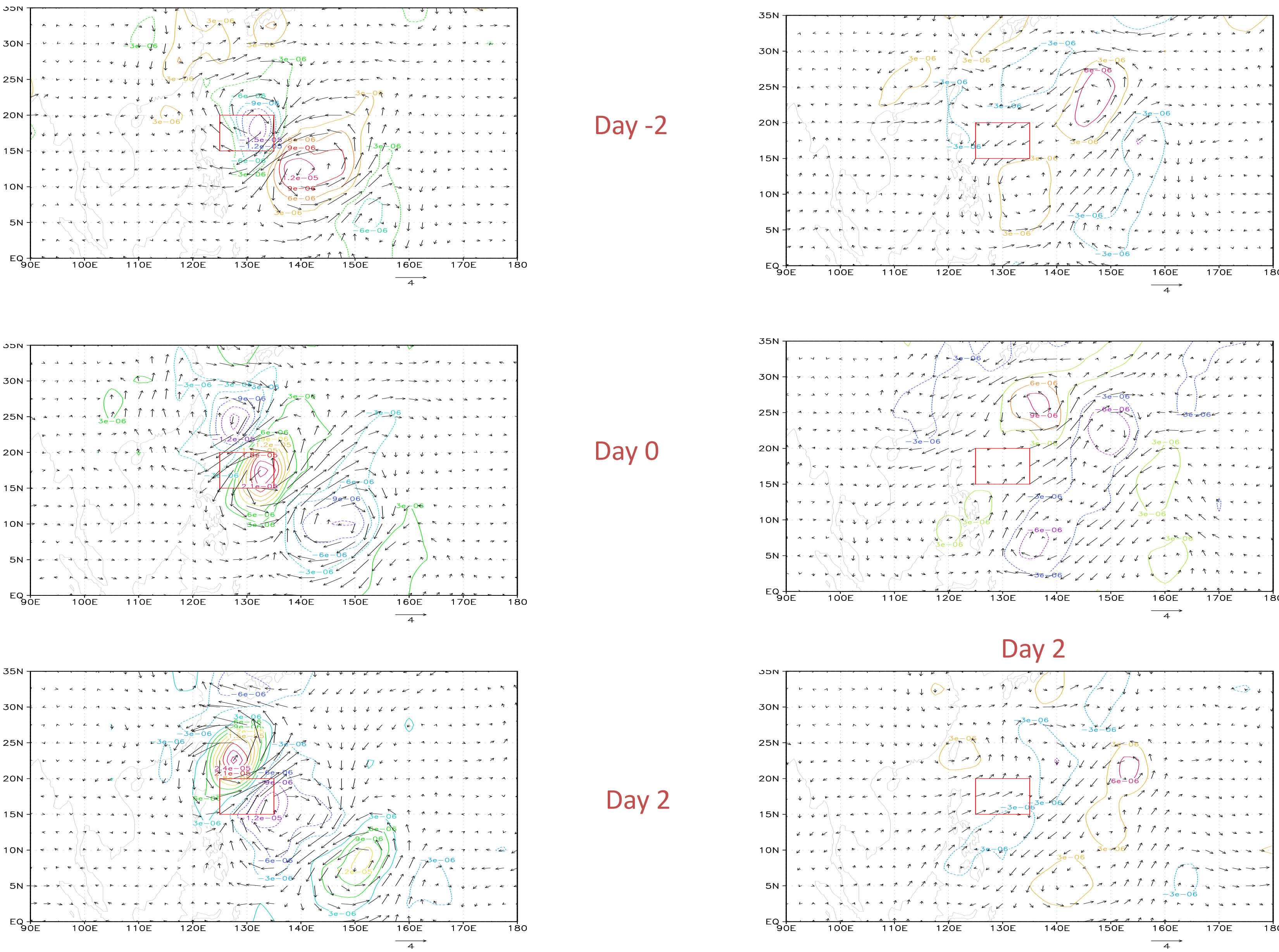

Energy conversion between eddy and LFBS (left) and between eddy and ISO(right)

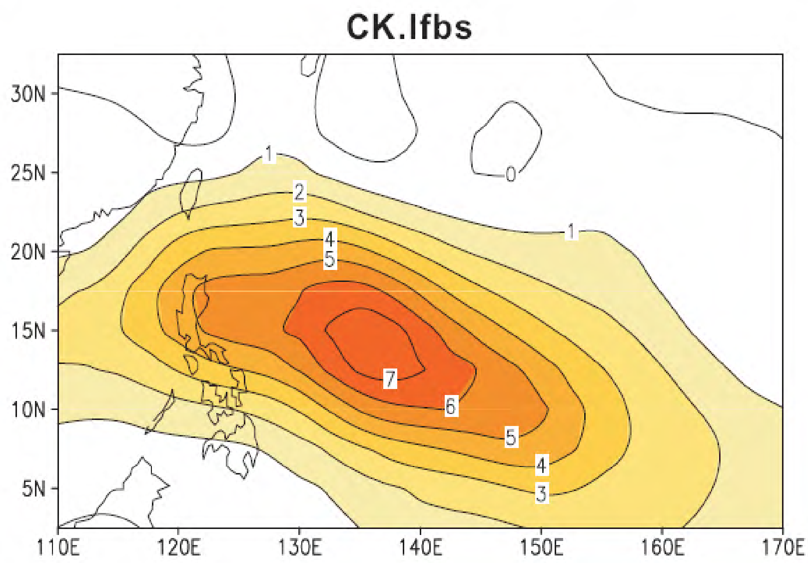

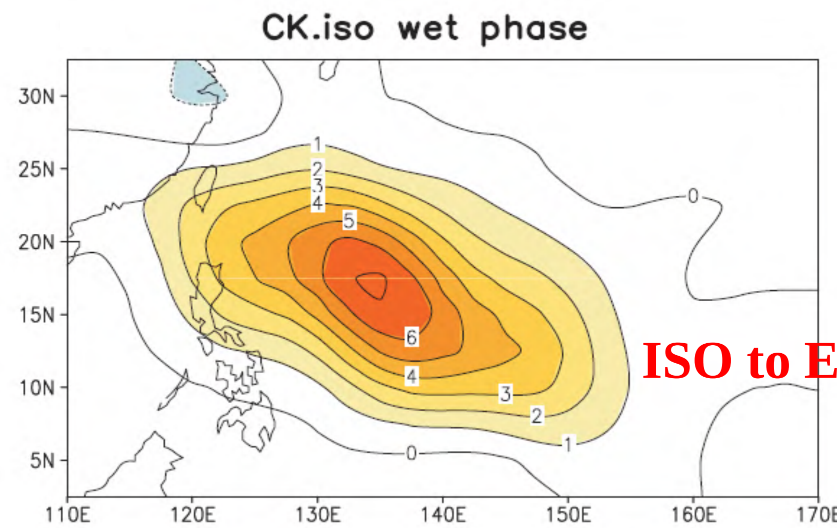

ISO to Eddy

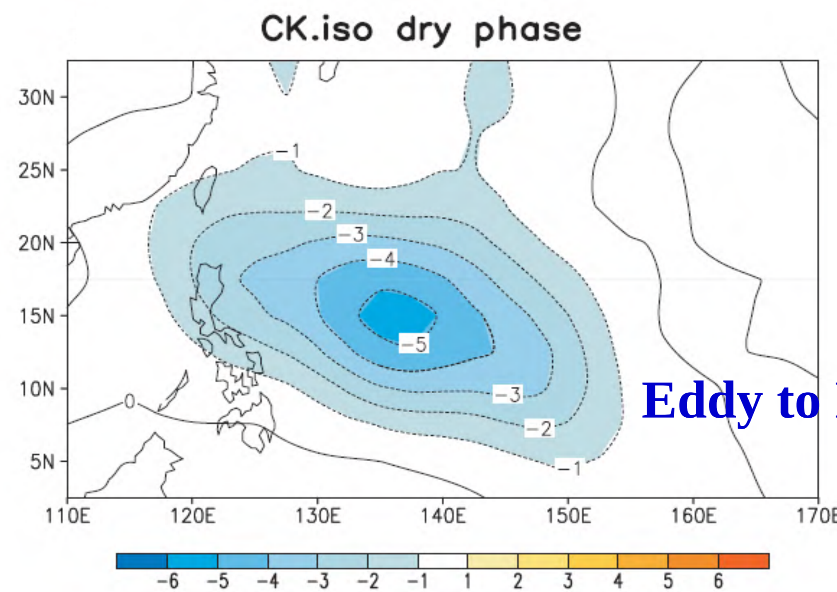

Eddy to ISO

$\overline{\overline{CK}}$ between LFBS and eddy always contributes **positively to the EKE** growth

ΔCK phase-dependent

Indicating an opposite energy conversion between ISO and synoptic-scale flows during ISO wet and dry phase

Hsu, Li, et al. 2011, J. Climate

A new EKE diagnosis method (Hsu, Li, et al. 2011)

1) A dependent variable may be separated into three components

$$A=\overline{\overline{A}}+\tilde{A}+A'$$

$\overline{\overline{A}}$ Low-frequency background state (**LFBS, >90days**)

$\tilde{A}$ **10-90-day ISO**

A' **3-10-day synoptic-scale disturbance**

2) By multiplying u′ and v′ in the both sides of the synoptic-scale momentum equations, one may derive the perturbation EKE equation.

$$\begin{aligned}
\frac{\partial K'}{\partial t} = & -u'\left(\frac{\partial \overline{\overline{u}}}{\partial t}+\frac{\partial \tilde{u}}{\partial t}\right)-v'\left(\frac{\partial \overline{\overline{v}}}{\partial t}+\frac{\partial \tilde{v}}{\partial t}\right) \\
& -u'(\overline{\overline{u}}+\tilde{u}+u')\left(\frac{\partial \overline{\overline{u}}}{\partial x}+\frac{\partial \tilde{u}}{\partial x}+\frac{\partial u'}{\partial x}\right)-v'(\overline{\overline{u}}+\tilde{u}+u')\left(\frac{\partial \overline{\overline{v}}}{\partial x}+\frac{\partial \tilde{v}}{\partial x}+\frac{\partial v'}{\partial x}\right) \\
& -u'(\overline{\overline{v}}+\tilde{v}+v')\left(\frac{\partial \overline{\overline{u}}}{\partial y}+\frac{\partial \tilde{u}}{\partial y}+\frac{\partial u'}{\partial y}\right)-v'(\overline{\overline{v}}+\tilde{v}+v')\left(\frac{\partial \overline{\overline{v}}}{\partial y}+\frac{\partial \tilde{v}}{\partial y}+\frac{\partial v'}{\partial y}\right) \\
& -u'(\overline{\overline{\omega}}+\tilde{\omega}+\omega')\left(\frac{\partial \overline{\overline{u}}}{\partial p}+\frac{\partial \tilde{u}}{\partial p}+\frac{\partial u'}{\partial p}\right)-v'(\overline{\overline{\omega}}+\tilde{\omega}+\omega')\left(\frac{\partial \overline{\overline{v}}}{\partial p}+\frac{\partial \tilde{v}}{\partial p}+\frac{\partial v'}{\partial p}\right) \\
& -u'\left(\frac{\partial \overline{\overline{\phi}}}{\partial x}+\frac{\partial \tilde{\phi}}{\partial x}+\frac{\partial \phi'}{\partial x}\right)-v'\left(\frac{\partial \overline{\overline{\phi}}}{\partial y}+\frac{\partial \tilde{\phi}}{\partial y}+\frac{\partial \phi'}{\partial y}\right)
\end{aligned}$$

$$\mathbf{K'=(u'^2+v'^2)/2}$$

3) Apply a **10-day low-pass filtering operator** (denoted by a single overbar) to the perturbation EKE equation, we have

$$\boxed{\frac{\partial \overline{K'}}{\partial t} = CK + CA + AM + AE + FG}$$

$$CK = -\overline{V'((\overline{\overline{V}}_3 + \tilde{V}_3 + V_3')\cdot\nabla_3)\overline{\overline{V}}} - \overline{V'((\overline{\overline{V}}_3 + \tilde{V}_3 + V_3')\cdot\nabla_3)\tilde{V}}$$

barotropic energy conversion from the LFBS and ISO flows to the synoptic-scale eddy

$$CA = -\frac{R}{p}\overline{T'\omega'}$$

baroclinic energy conversion from EAPE to EKE

$$AM = AMm + AMi = -\overline{\overline{\overline{V}}_3\cdot\nabla_3 K'} - \overline{\tilde{V}_3\cdot\nabla_3 K'}$$

advections of EKE by both the LFBS (AMm) and the ISO (AMi) flows

$$AE = -\overline{V_3'\cdot\nabla_3 K'}$$

advection of EKE by the synoptic-scale eddy

$$FG = -\overline{\nabla_3\cdot(V'\phi')}$$

convergence of eddy geopotential flux

CK and AM terms explicitly reflect the eddy-mean flow interactions.

CA, AE, FG terms reflect the eddy-eddy interactions.

Strategy to isolate the ISO-SSV interaction

$$\frac{\partial \overline{K'}}{\partial t} = CK + CA + AM + AE + FG \qquad \text{(a)}$$

The left hand side consists of the sum of the EKE tendencies on both the LFBS and ISO timescales

1) Applying a **90-day low-pass filter**, one may derive LFBS EKE tendency eq. :

$$\frac{\partial \overline{\overline{K'}}}{\partial t} = \overline{\overline{CK}} + \overline{\overline{CA}} + \overline{\overline{AM}} + \overline{\overline{AE}} + \overline{\overline{FG}} \qquad \text{(b)}$$

2) **Subtracting** the LFBS EKE tendency from Eq.(a), one may derive the time change rate of **EKE on the intraseasonal timescale:**

$$\boxed{\frac{\partial \tilde{K}'}{\partial t} = \Delta CK + \Delta CA + \Delta AM + \Delta AE + \Delta FG}$$

$$\Delta(\ ) = (\ ) - \overline{\overline{(\ )}}$$

△ CK (shading) results from **NE-SW tilted SSV interacting with** **ISO flow (vector)**

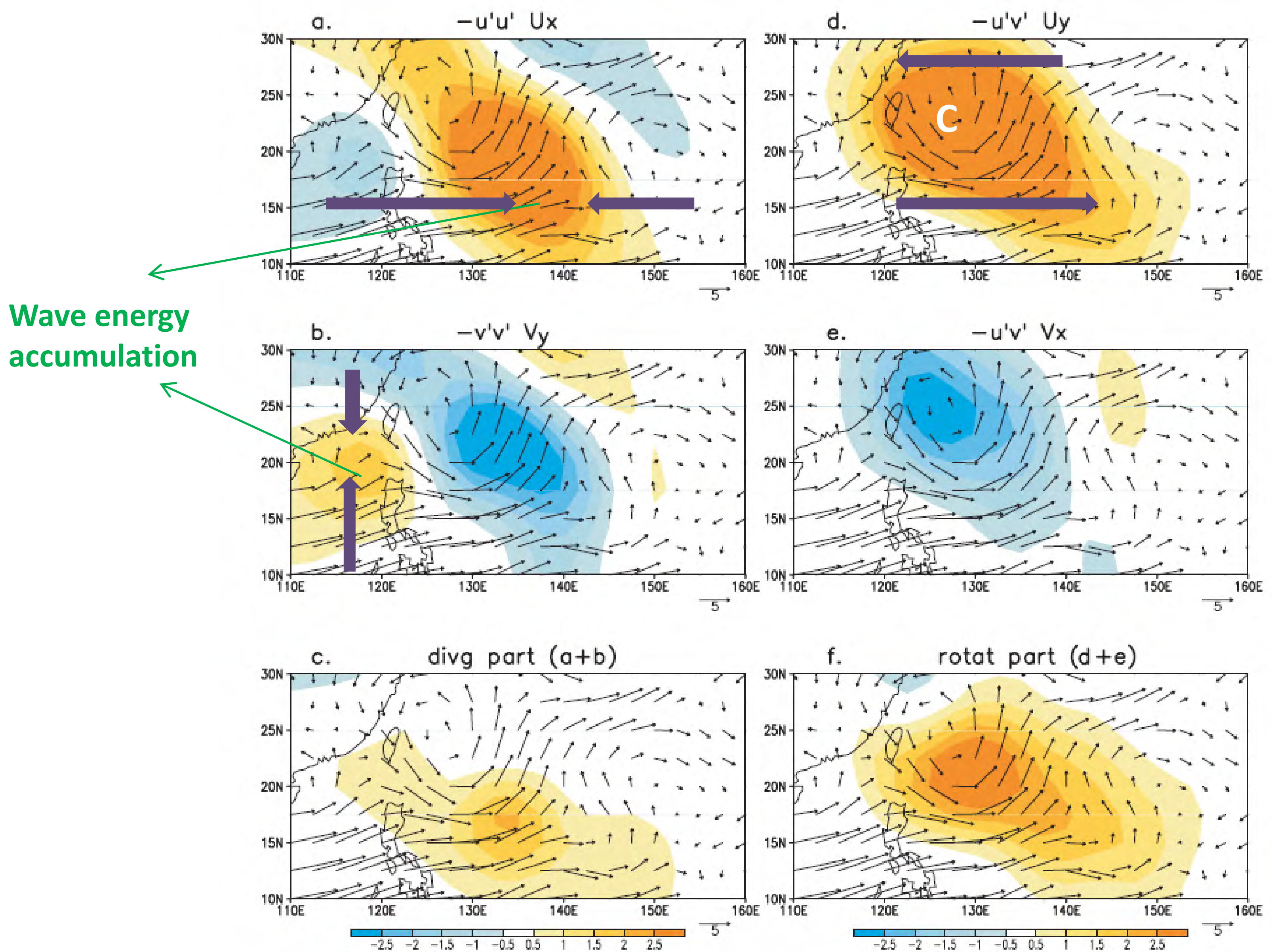

Hsu, Li, et al. 2011, JC

Both **divergent** and **rotational** ISO flows contribute to enhanced CK during ISO wet phase

Relationship between the barotropic energy conversion (CK) and the TC genesis

shading : total $CK=\overline{\overline{CK}}+\Delta CK$ dot : TC genesis location

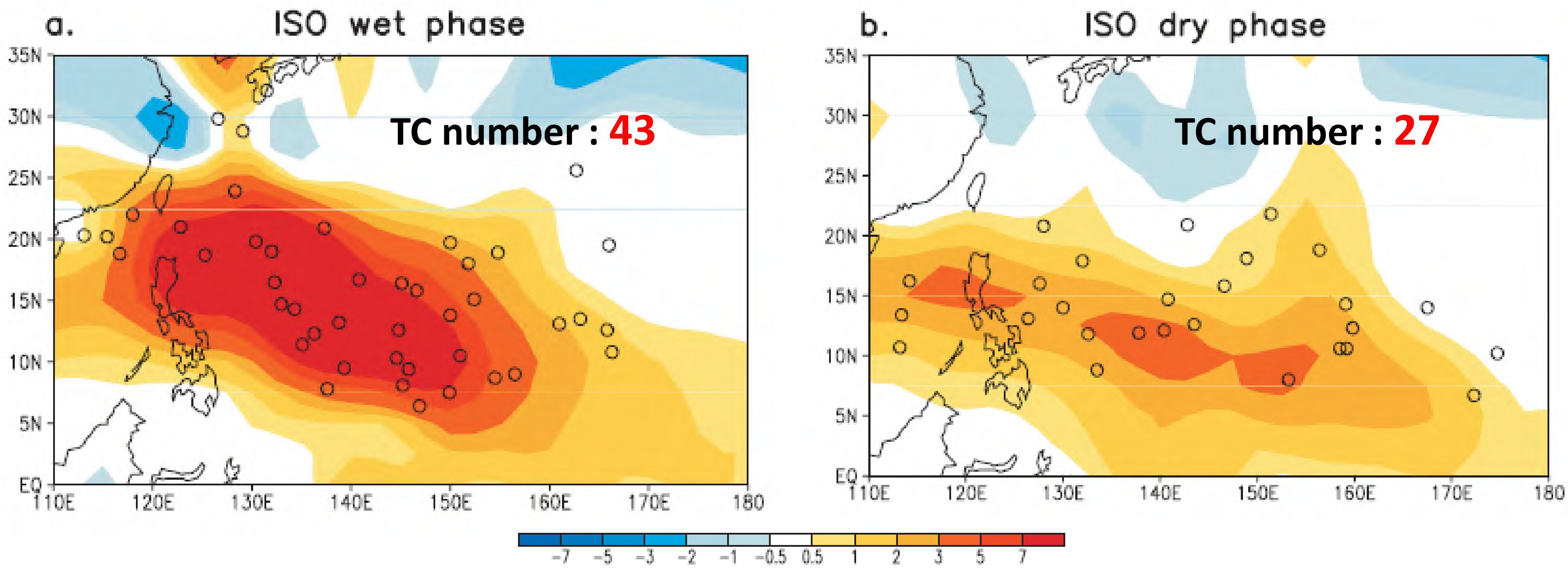

1) Enhanced CK favors the development of synoptic seed disturbances, some of which eventually grow into TCs.

2) TC genesis number during the ISO wet phase is about **1.5 times greater** than that during the ISO dry phase.

- **What is the relative importance of the ISO dynamic and thermodynamic fields in affecting TC development?**

Cao, X., **T. Li**, M. Peng, W. Chen, and G. H. Chen, 2014, Effects of the monsoon trough intraseasonal oscillation on tropical cyclogenesis over the western North Pacific, *J. Atmos.* Sci., 71, 4639-4660.

Model and experimental design—— large-scale flow field, model configuration and bogus vortex

Vt

Active: solid

Inactive: dashed

Div

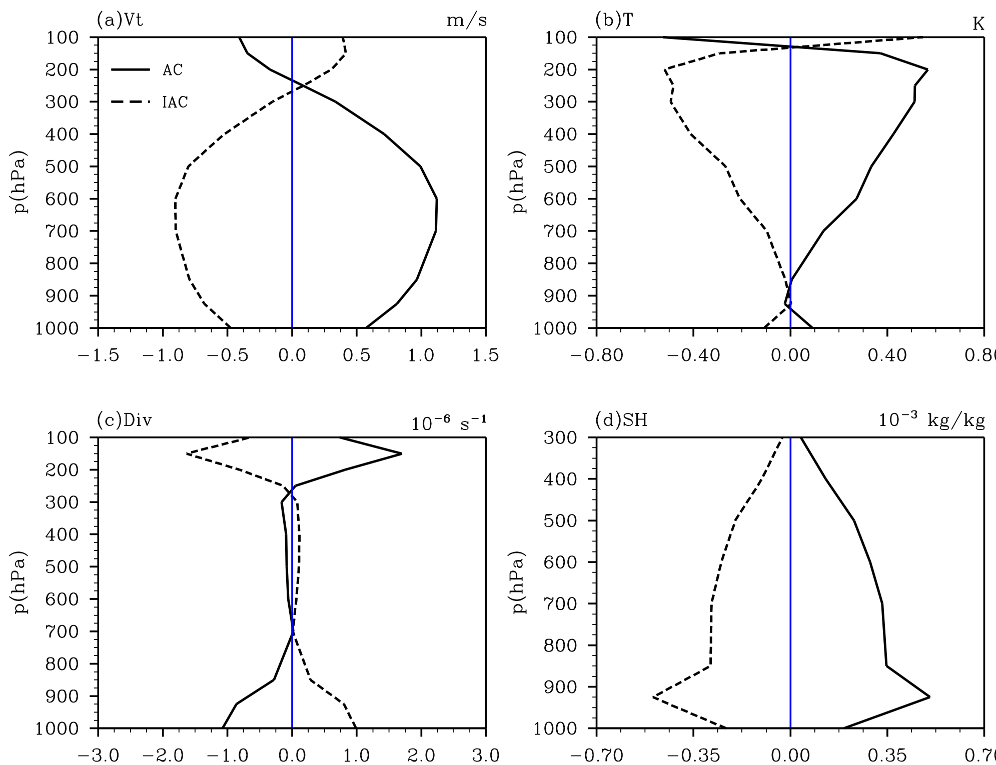

T

Reanalysis data

Sh

- Triply nested. Horizontal resolution of 27, 9 and **3** km.
- **Beta-plane** (15∘**N**) and **a quiescent environment** with **constant SST** (29∘C).
- A **fixed lateral boundary** condition.
- **A weak initial balanced axisymmetric vortex**. Vm= 8 m/s, RMW= 150 km
- The vorticity **maximum is at the surface** and decreases upward (Wang 1995, 2001)

Model and experimental design—— experimental design

The list of numerical experiments

	Group 1	Group 2		Group 3	
Beta plane	**CTL**	**ACV**	**AC**	**IACV**	**IAC**
MT ISO	**No**	**Active**	**Active**	**Inactive**	**Inactive**
Vortex	**Yes**	**Yes**	**No**	**Yes**	**No**

To examine "pure" vortex evolutions, background ISO fields need to be removed.

ACV:

ISO AC

+ Vortex

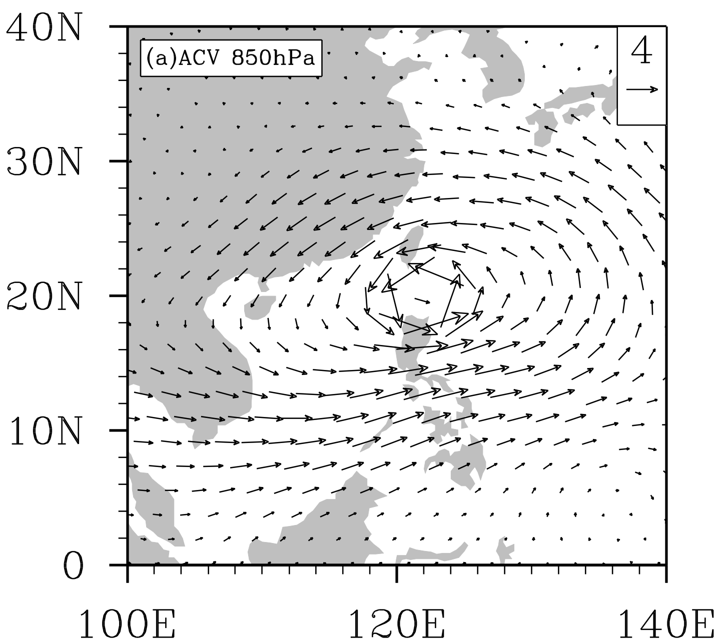

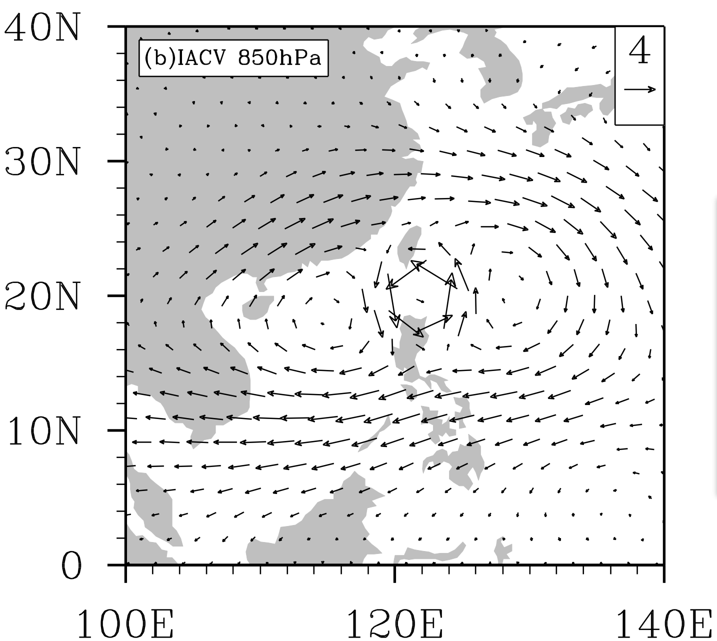

IACV:

ISO IAC

+ Vortex

ISO impact on vortex development

Time evolution of (a) the **minimum sea level pressure** (unit: hPa) and (b) the **maximum azimuthal mean wind speed** (unit: m s^{-1}) at 10 m in the three experiments **CTL** (**black solid line**), **ACV** (**red dashed line**) and **IACV** (**blue dotted line**).

MSLP

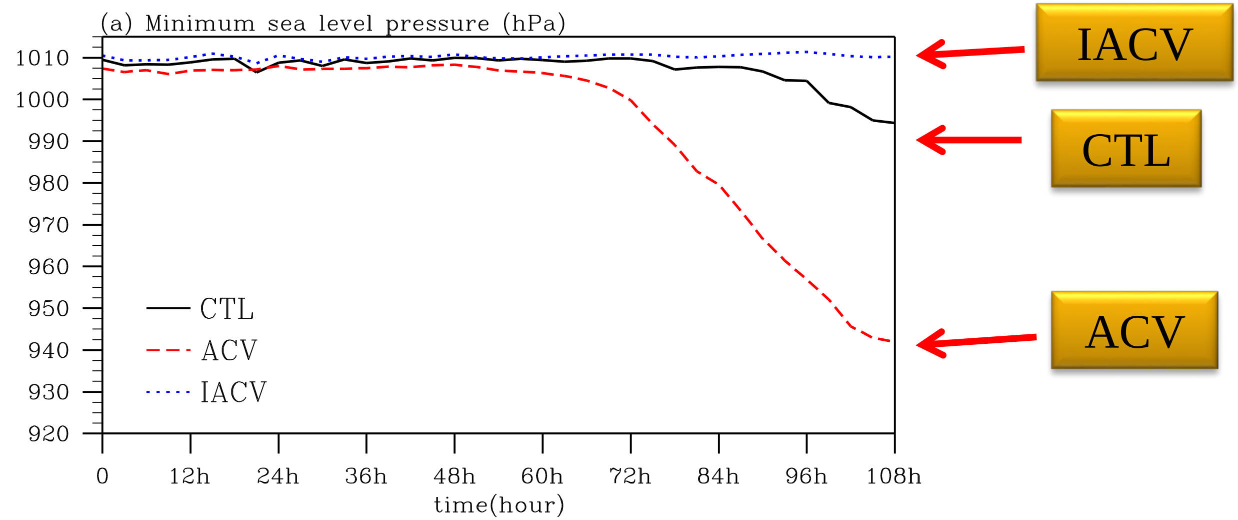

MAMW

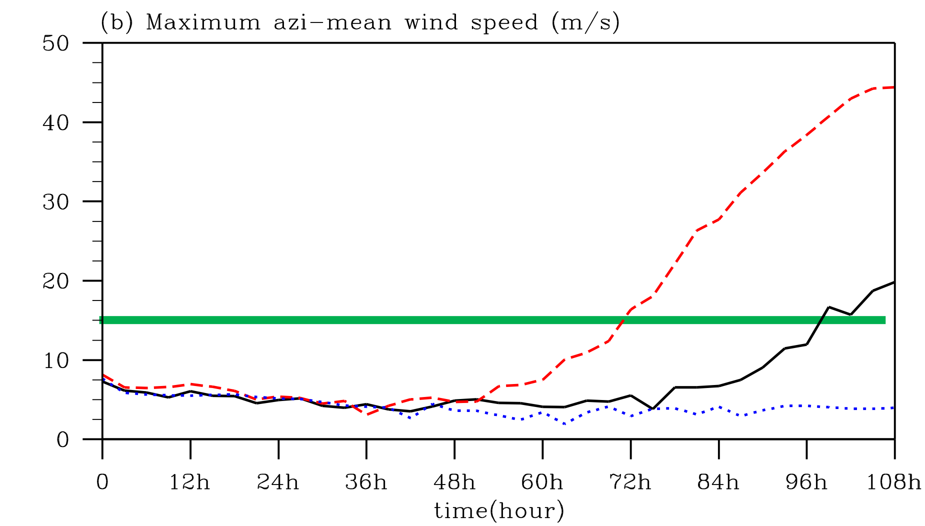

Define:15 m/s

t = 99h CTL

t = 72h ACV

ISO impact on vortex development

1h　　3h　　5h　　7h

Radial wind

Tangential wind

Geopotential

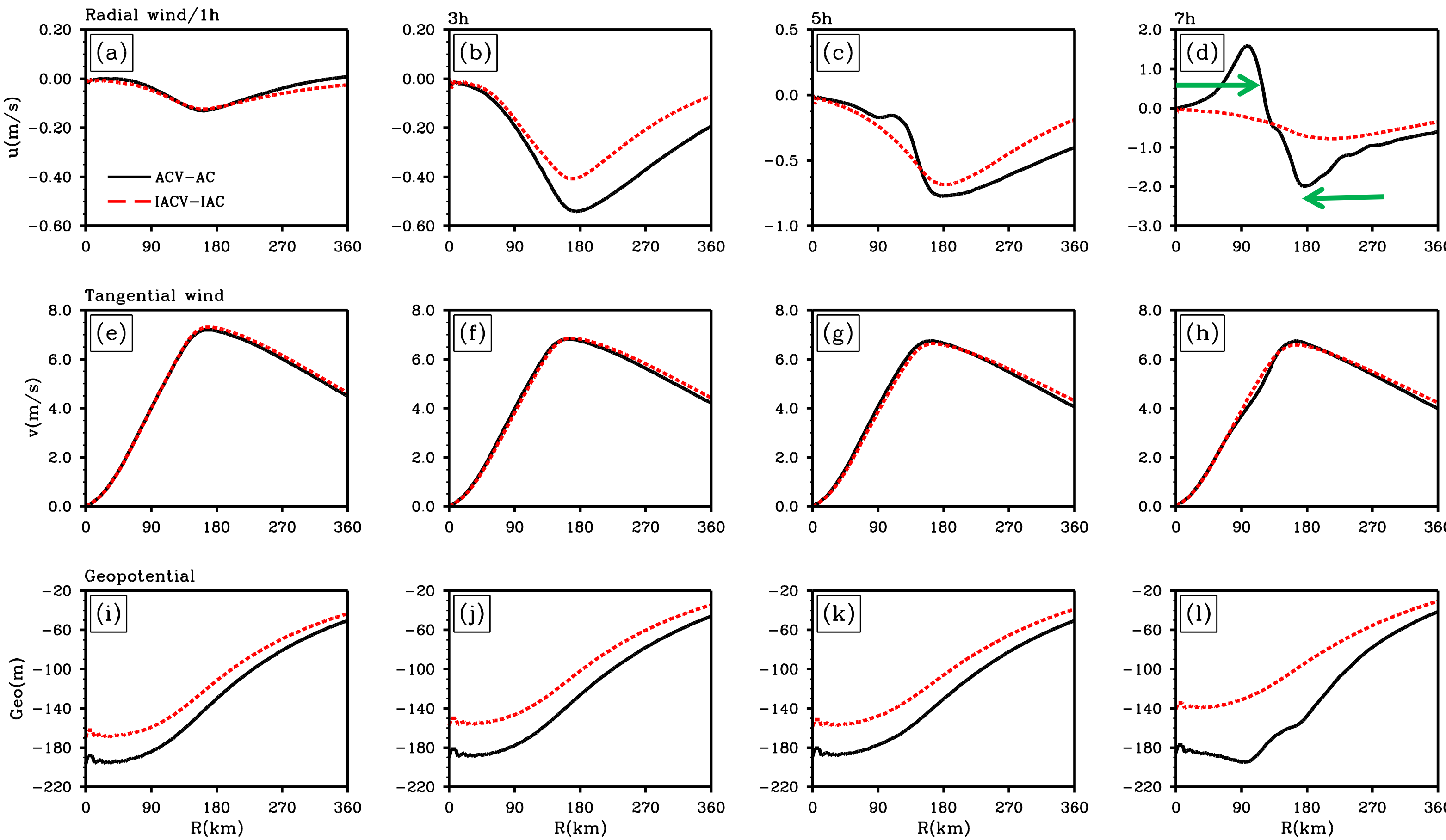

Black: active
Red : inactive

1000 hPa

ISO impact on vortex development

Radial wind

1h 3h 5h 7h

Active

Inactive

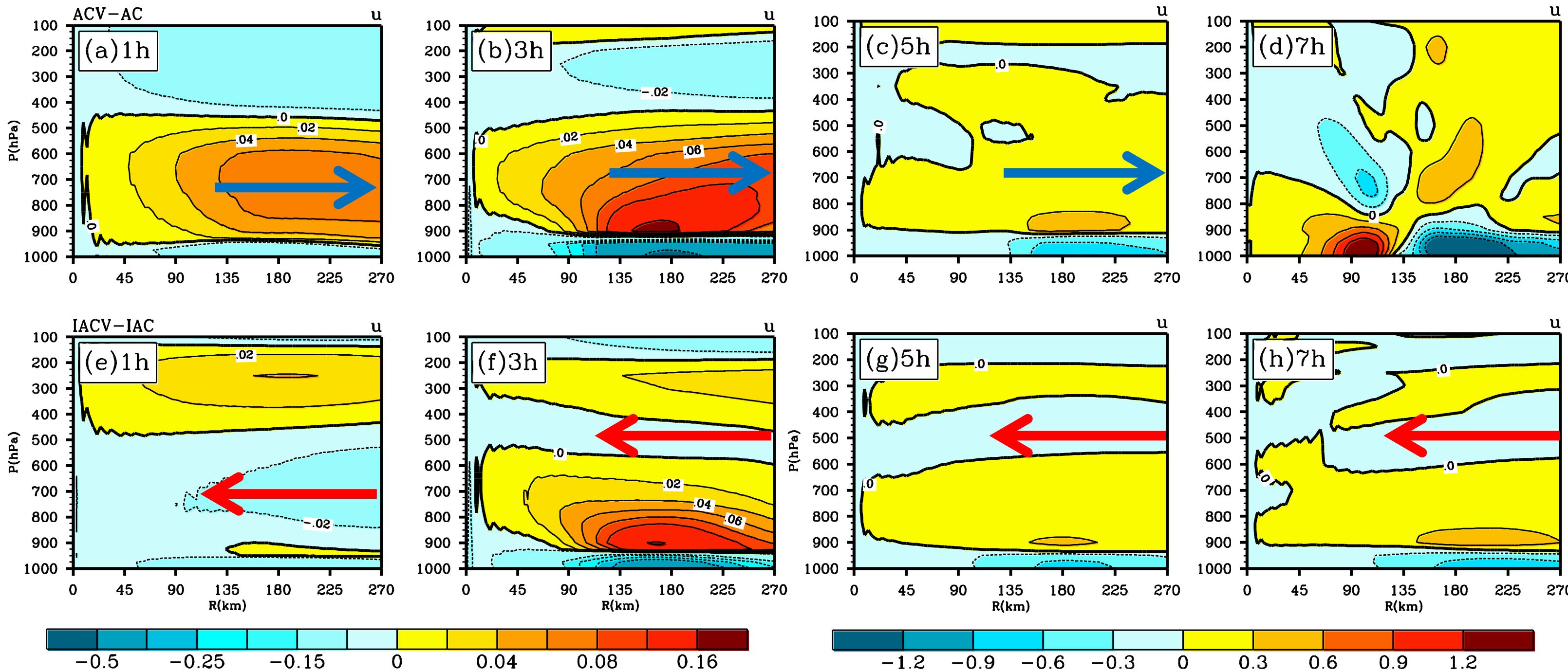

$$\frac{\partial u'}{\partial t} = -\left(\bar{u}\frac{\partial u'}{\partial r} + u'\frac{\partial \bar{u}}{\partial r} + u'\frac{\partial u'}{\partial r}\right) - \left(\frac{\bar{v}}{r}\frac{\partial u'}{\partial \lambda} + \frac{v'}{r}\frac{\partial \bar{u}}{\partial \lambda} + \frac{v'}{r}\frac{\partial u'}{\partial \lambda}\right) - \left(\bar{w}\frac{\partial u'}{\partial p} + w'\frac{\partial \bar{u}}{\partial p} + w'\frac{\partial u'}{\partial p}\right)$$

$$+\left(f_0 v' + \frac{v'^2}{r}\right) + \boxed{\frac{2v'\bar{v}}{r}} - \frac{\partial \Phi'}{\partial r} + F_u'$$

The overbar are ISO wind. The prime is vortex perturbation wind.

ISO impact on vortex development

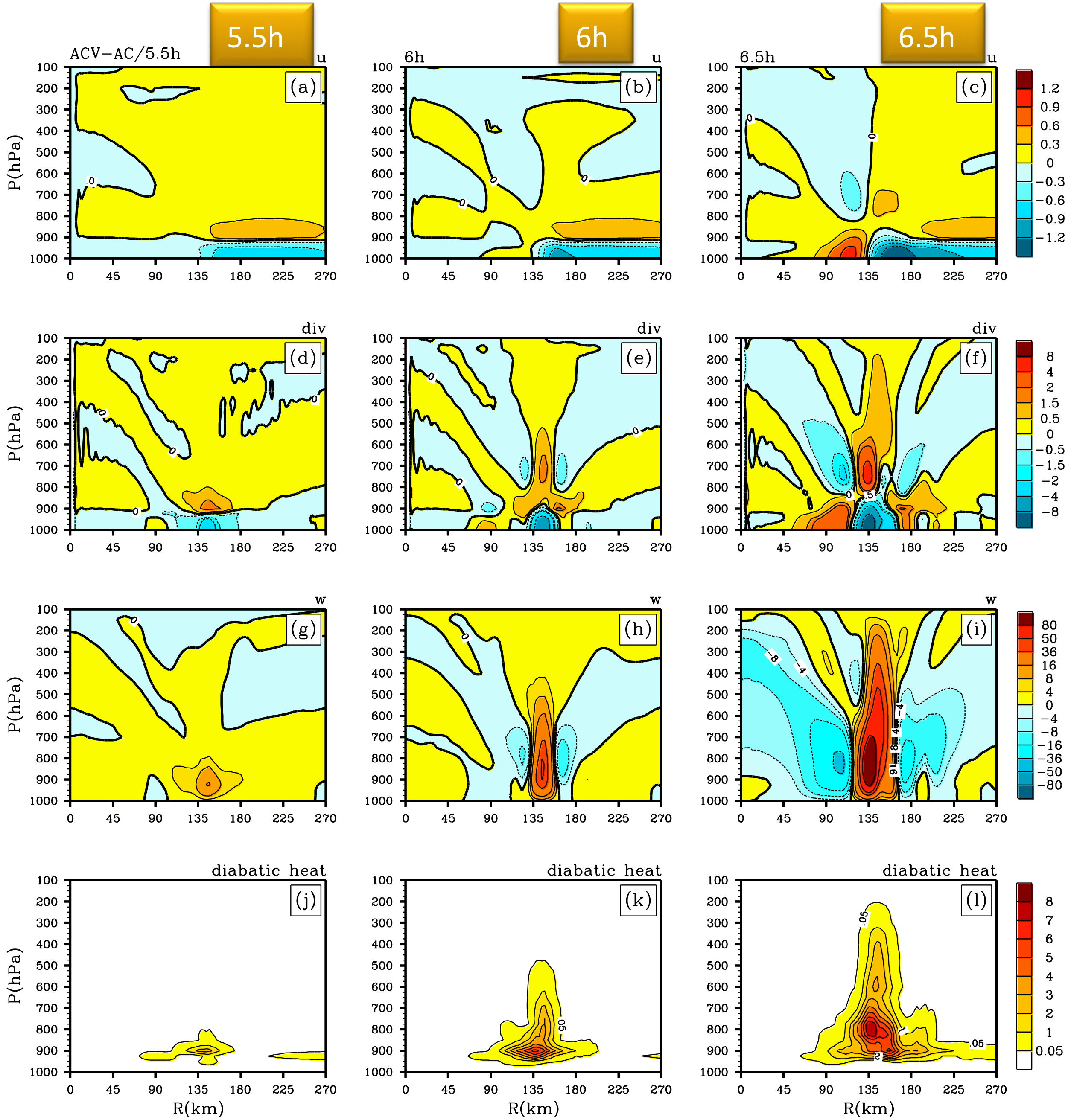

Active

Radial wind

Div

W

heating

ISO impact on vortex development

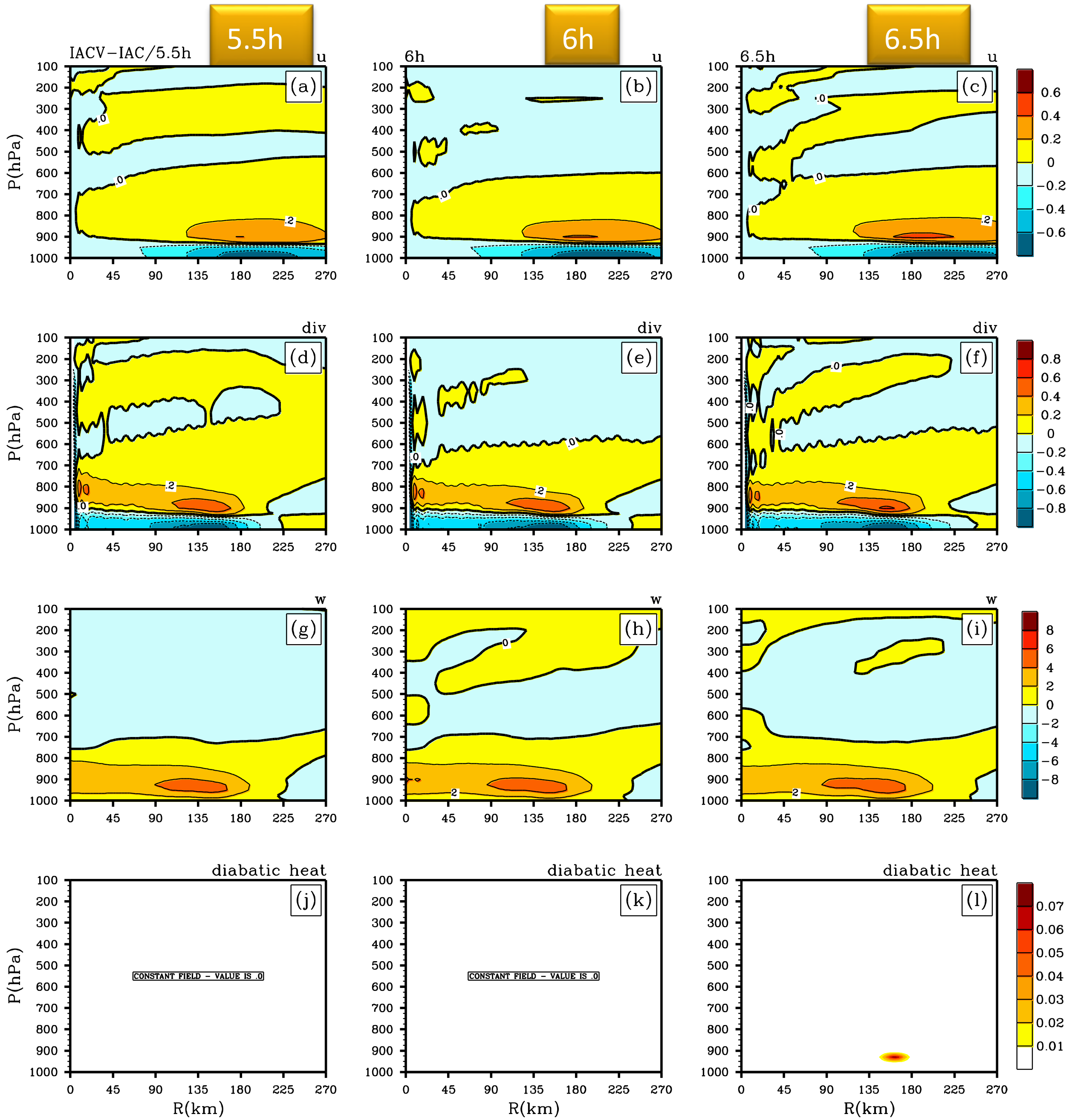

Inactive

Radial wind

Div

W

heating

Relative roles of ISO dynamic and thermodynamic impacts

The list of sensitivity experiments

	Group 1		Group 2	
Beta plane	ACV_NOSH	AC_NOSH	ACV_SH	AC_SH
MT ISO	Active	Active	Active	Active
Variables	u, v, ps, T, hgt	u, v, ps, T, hgt	sh	sh
Vortex	Yes	No	Yes	No

"NOSH" denotes prescribed ISO dynamic fields but no moisture field; "SH" denotes prescribed ISO moisture field but no dynamic fields.

Time evolution of (a) the minimum sea level pressure (unit: hPa) in the four experiments CTL, ACV, ACV_SH and ACV_NOSH.

MSLP

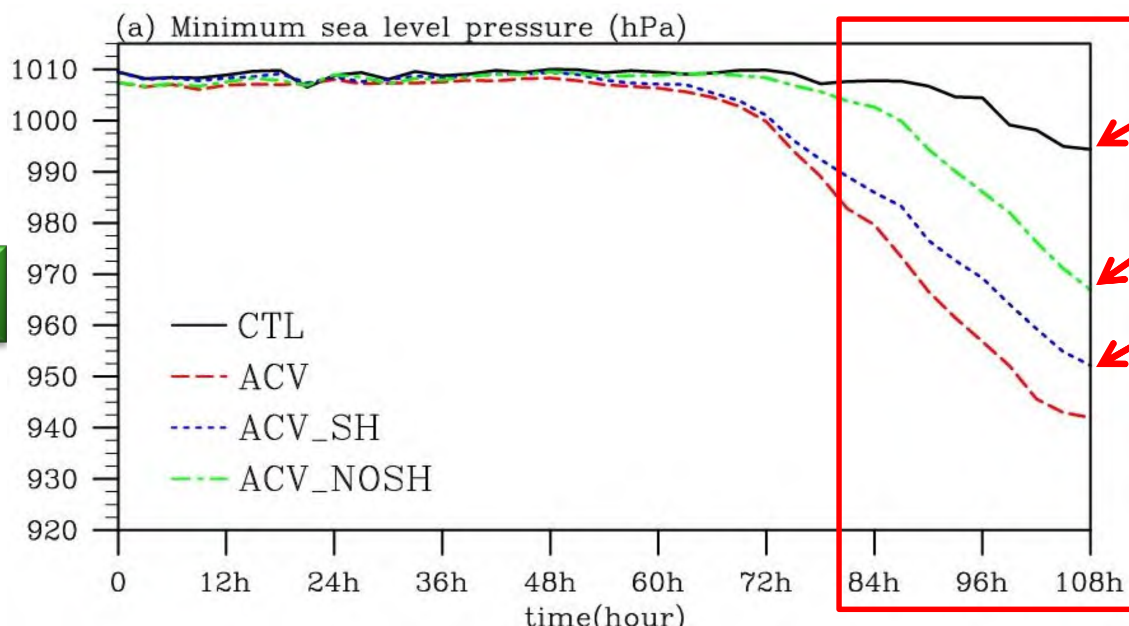

CTL

ACV_NOSH

ACV_SH

2:1

Relative roles of ISO dynamic and thermodynamic impacts

CTL

5h

7h

9h

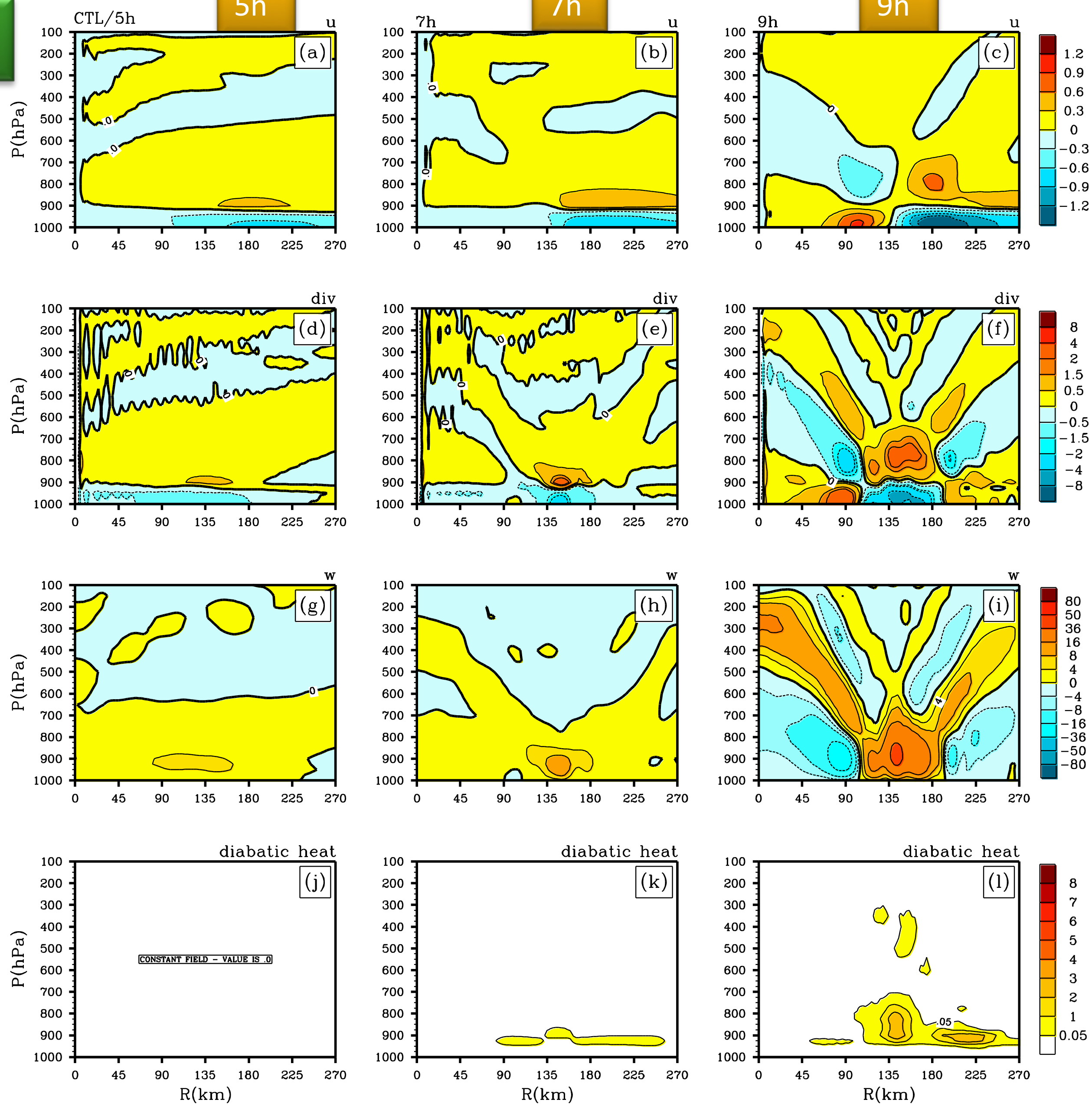

Radial wind

Div

W

heating

Relative roles of ISO dynamic and thermodynamic impacts

NOSH

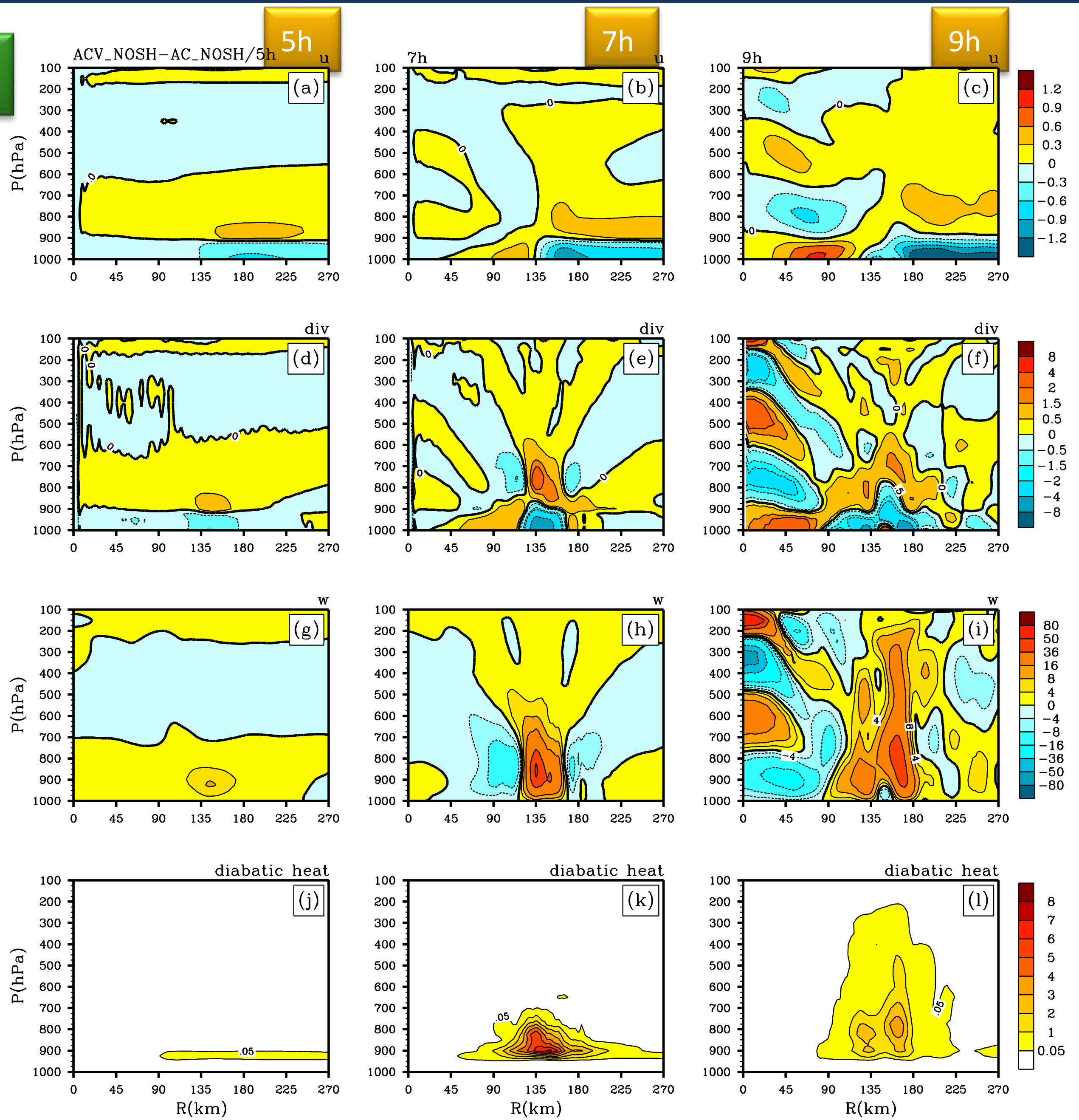

Radial wind

Div

W

heating

Relative roles of ISO dynamic and thermodynamic impacts

SH

5h

7h

9h

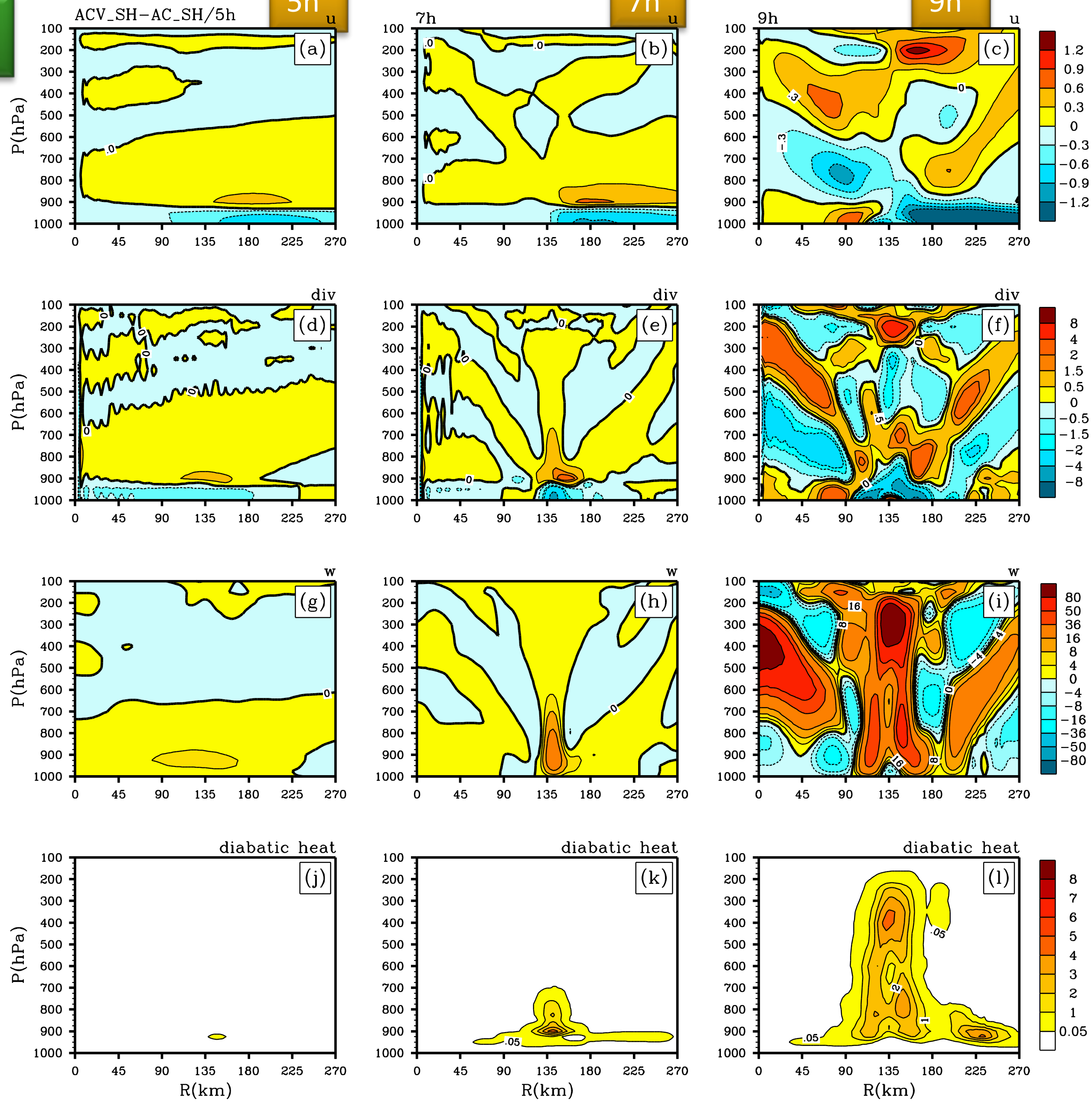

Radial wind

Div

W

heating

Relative roles of ISO dynamic and thermodynamic impacts

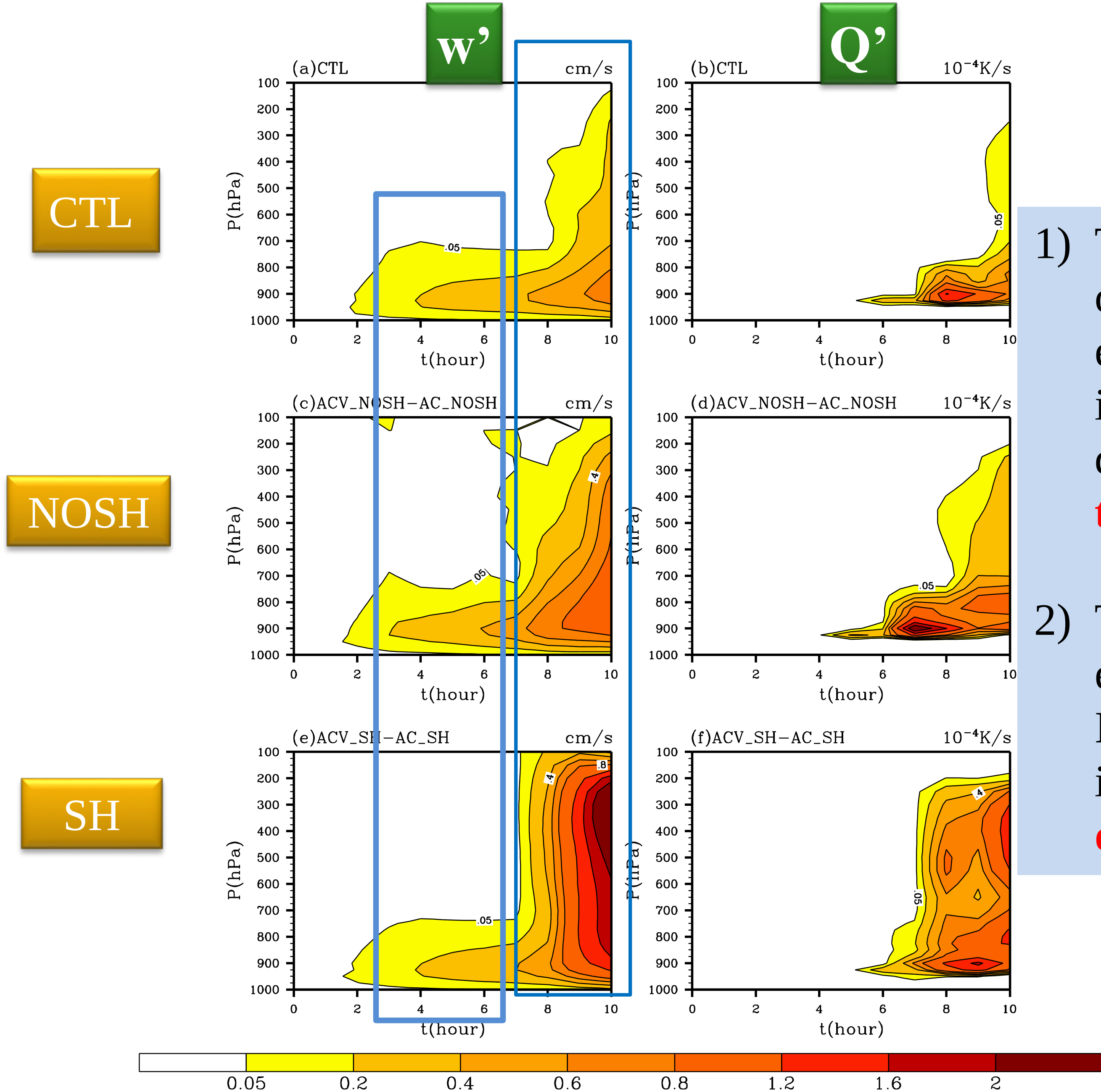

1) The **dynamic factors** of the active ISO exert a **greater** impact on the vortex development **during the initial 6 hours**.

2) The **thermodynamic** effect of the active ISO becomes more important **in the later development stage**.

Relative roles of ISO dynamic and thermodynamic impacts

Inactive experiments

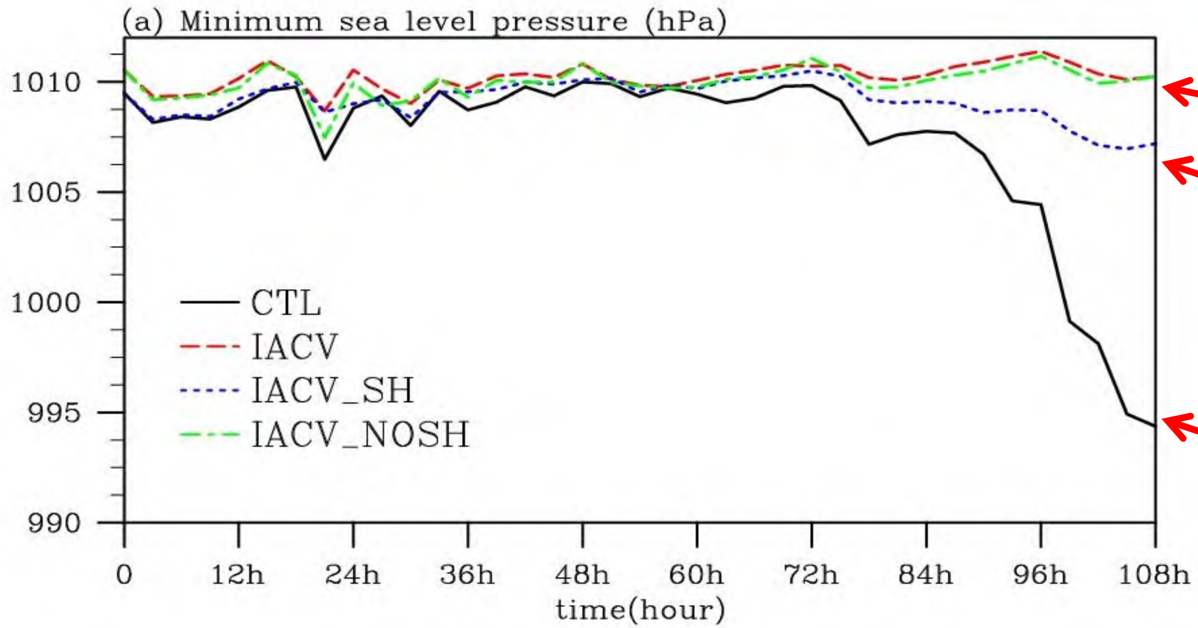

IACV_NOSH

IACV_SH

CTL

In a mixed manner

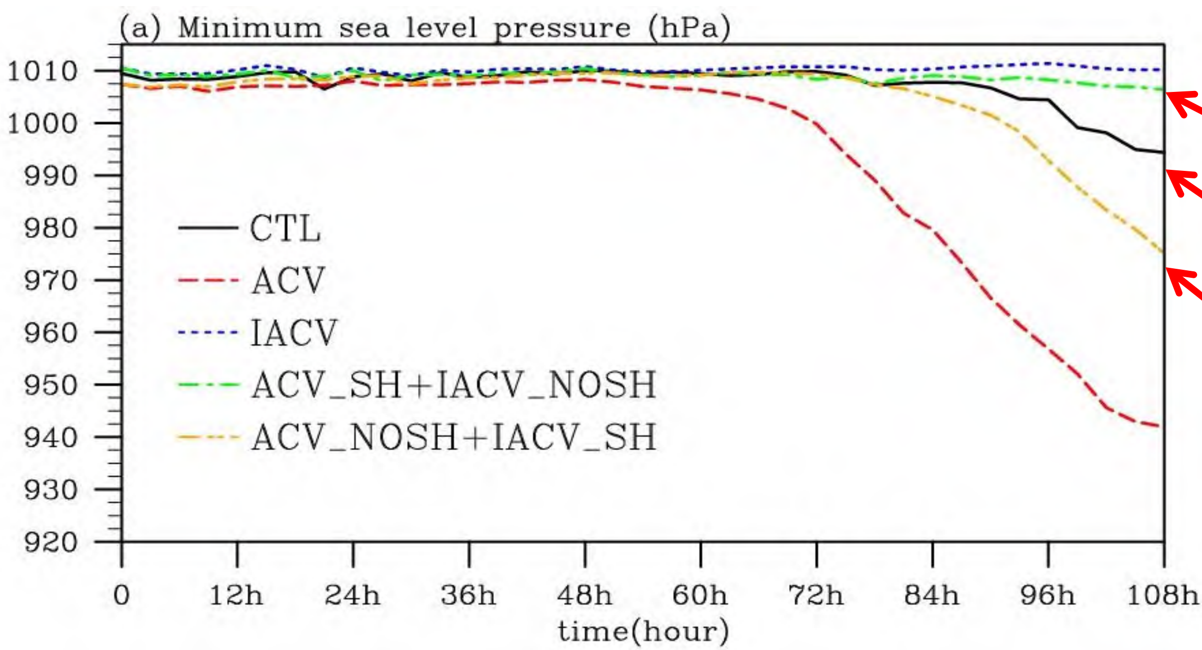

ACV_SH+ IACV_NOSH

CTL

ACV_NOSH+ IACV_SH

Summary

1) ISO modulates TC genesis through both dynamic and thermodynamic processes.

a. **Dynamic processes: Interactions** between ISO-scale and vortex-scale cyclonic flows during ISO active phase lead to the generation of **vortex-scale outflow at mid-level,** which helps upward lifting of friction-induced ascending motion and thus upward moisture transport. **Interactions** between ISO-scale anticyclonic flow and vortex-scale cyclonic flow during ISO inactive phase lead to the generation of **vortex-scale inflow at mid-level,** which prohibits friction-induced ascending motion and thus suppresses TC development.

b. Thermodynamic process: **A greater background specific humidity associated with active ISO** promotes earlier and stronger TC development.

2) The ISO thermodynamic impact is about two times as large as that of the dynamic impact during active phase of ISO**.**

3) The dynamic impact of the anticyclonic flow during inactive ISO phase **inhibits TC development in the absence of the summer mean flow.**